学　位　論　文

Doctor's Thesis

論文題名：Role of Reactive Oxygen Species in Tumor: Enhanced Antitumor Effect by Focused Radical Generation in Solid Tumor
（活性酸素と癌：固型腫瘍標的化ラジカル生成と癌治療）

著者名：　方　軍
Fang Jun

指導教官名：　微生物学講座教授
前田　浩

審査委員名：１）分子遺伝学講座担当教授　森　正敬
２）腫瘍医学講座担当教授　佐谷秀行
３）生化学第一講座担当教授　三浦　洌
４）薬理学第二講座担当教授　西　勝英

２００３年３月

Role of Reactive Oxygen Species in Tumor: Enhanced Antitumor Effect by Focused Radical Generation in Solid Tumor

Doctor's Thesis By

Fang Jun

For the Fulfillment of the Doctorate Degree in Medical Science

Under supervision of

Professor Hiroshi Maeda, M.D., Ph.D

Associate Professor Takaaki Akaike, M.D., Ph.D

Assistant Professor Tomohiro Sawa, Ph.D

Department of Microbiology
Kumamoto University Graduate School of Medicine
Honjo 2-2-1, Kumamoto 860-0811, Japan

March, 2003

CONTENTS

ABSTRACT

Reactive oxygen species (ROS), e.g., superoxide anion ($O_2^{\cdot}$), hydrogen peroxide (H_2O_2), and hydroxyl radical (•OH), are potentially harmful by-products of normal cellular metabolism that directly affect cellular functions (e.g., development, growth and aging) and survival as well as causing mutation. ROS are generated by all aerobic organisms and seem to be indispensable for signal transduction pathways that regulate cell growth and reduction-oxidation (redox) status. However, overproduction of these highly reactive oxygen metabolites can initiate lethal chain reactions, which involve oxidation and damage to structures that are crucial for cellular integrity and survival. In fact, many antitumor agents, such as vinblastine, *cis*platin, mitomycin C, doxorubicin, camptothecin, and inostamycin exhibit antitumor activity via ROS-dependent activation of apoptotic cell death, suggesting potential use of ROS as an antitumor principle. In this study, the potential role of ROS was investigated for treating solid tumors, via selectively inducing ROS to solid tumors directly, or inhibiting the antioxidative enzyme of tumor cells, or by combination of both.

To induce the exogenous ROS to solid tumors, an H_2O_2-generating enzyme, D-amino acid oxidase (DAO) was selected, and was conjugated with polyethylene glycol (PEG) (PEG-DAO) for targeting tumor. Compared with native DAO, PEG-DAO showed improved pharmacokinetic parameters in mice after i.v. injection. PEG-DAO administered i.v. accumulated selectively in tumor tissue with insignificant accumulation in normal organs and tissues, by virtue of the EPR (enhanced permeability and retention) effect that is commonly observed in solid tumors for biocompatible macromolecular drugs. To generate cytotoxic H_2O_2 at the tumor site, PEG-DAO was first administrated i.v. to tumor-bearing mice. After an adequate lag time, the substrate of DAO, D-proline, was injected i.p.. This treatment resulted in significant suppression of tumor growth compared with that of control animals (not given treatment) ($P < 0.001$). Oxidative metabolites were significantly increased in solid tumors by administration of PEG-DAO followed by D-proline ($P < 0.002$, compared with the group receiving no treatment), as evidenced by thiobarbituric acid-reactive substance assay. This treatment did not affect results from the metabolites in the liver and kidney. In addition, no loss of body weight in mice was observed at the therapeutic dose.

Heme oxygenase-1 (HO-1) has been considered to be an important antioxidative

enzyme for cytoprotection against free radicals in solid tumor. High expression of the HO-1 is now well known in solid tumors in humans and experimental animal models. Previously report showed that HO-1 may be involved in tumor growth (Tanaka et al. Br. J. Cancer. 2003. in press), in that inhibition of HO activity in tumors by using zinc protoporphyrin (ZnPP) significantly reduced tumor growth in a rat model. In this study, I demonstrated that poly(ethylene glycol)-conjugated ZnPP (PEG-ZnPP), a water-soluble derivative of ZnPP. exhibited potent HO inhibitory activity and had an antitumor effect *in vivo*. *In vitro* studies with cultured SW480 cells. which express HO-1, showed that PEG-ZnPP induced oxidative stress. and consequently apoptotic death. of these cells. Pharmacokinetic analysis revealed that PEG-ZnPP administered i.v. had a circulation time in blood that was 40 times longer than that for nonpegylated ZnPP. More important, PEG-ZnPP preferentially accumulated in solid tumor tissue in a murine model by taking advantage of the EPR effect. *In vivo* treatment with PEG-ZnPP (equivalent to 1.5 or 5 mg of ZnPP/kg. i.v.. injected daily for 6 days) remarkably suppressed the growth of S180 tumors implanted in the dorsal skin of ddY mice without any apparent side effects. In addition, this PEG-ZnPP treatment produced tumor-selective suppression of HO activity as well as induction of apoptosis. These findings suggest that tumor-targeted inhibition of HO activity could be achieved by using PEG-ZnPP. which induces apoptosis in solid tumors. probably through increased oxidative stress.

Furthermore, the combined effect of these two compounds was investigated. In *in vitro* study. combination of hydrogen peroxide (H_2O_2) and PEG-ZnPP induced significant increase of intracellular oxidative stress; compared with untreated control cells (apoptotic cells of 2.69% in total counted cells), 44.08% cells showed apoptotic change in combination treatment group, whereas only 10.23% and 10.21% cells were found apoptosis in H_2O_2 treatment group and PEG-ZnPP treatment group. respectively. In *in vivo* study, 24 h after one injection of PEG-ZnPP (equivalent to 1.5 mg ZnPP/kg, i.v.). administration of PEG-DAO system (PEG-DAO 0.75 U/mouse. i.v. followed by its substrate D-proline 0.5 mmol/mouse. i.p. 4 h after PEG-DAO injection, daily for 3 days) resulted in significant suppression (> 90%) of tumor growth. compared with that of untreated control animals ($P < 0.01$). Whereas, either PEG-DAO system or PEG-ZnPP alone showed little suppression of tumor growth under the same treatment condition. TUNEL assay showed that apoptotic cells markedly increased in solid tumors by

combined administration of PEG-DAO and PEG-ZnPP ($P < 0.001$, compared with untreated control group). These results suggest the synergistic effect of PEG-ZnPP and PEG-ZnPP system, which may be extended to many conventional anticancer drugs that generate ROS. Moreover, no apparent side effects were found in this treatment, evidenced by body weight change, blood counts and blood chemistry, and tissue histological examination of the treated animals.

Taken together, these findings show the therapeutic potential of cytotoxic ROS generated in solid tumors. It was also confirmed that polymer conjugation makes highly efficient tumor targeting possible, thus antitumor effect is obtained through the increased ROS in tumor site based on the EPR effect. Consequently, remarkable antitumor activity had been achieved by selectively delivering DAO system to tumor, as well as inhibiting HO-1 activity in tumor, and then combination of both, via an apoptosis-dependent pathway.

LIST OF PUBLICATIONS

1. Fang, J., Sawa, T., Akaike, T., and Maeda, H. Tumor-targeted Delivery of Polyethylene Glycol-conjugated D-Amino Acid Oxidase for Antitumor Therapy via Enzymatic Generation of Hydrogen Peroxide. Cancer Res. 62(11):3138-43, 2002.

2 Sahoo, S. K., Sawa, T., Fang, J., Tanaka, S., Miyamoto, Y., Akaike, T., and Maeda, H. Pegylated zinc protoporphyrin: a water-soluble heme oxygenase inhibitor with tumor-targeting capacity. Bioconjug Chem. 13(5):1031-8, 2002.

3 Tanaka, S., Akaike, T., Fang, J., Beppu, T., Ogawa, M., Tamura, F., Miyamoto, Y., and Maeda, H. Antiapoptotic effect of haem oxygenase-1 induced by nitric oxide in experimental solid tumour. Br. J. Cancer 2003, in press.

4 Tanaka, T., Akaike, T., Wu, J., Fang, J., Sawa, T., Ogawa, M., Beppu, T., and Maeda, H. Modulation of tumor-selective vascular blood flow and extravasation by the stable prostaglandin I_2 analogue beraprost sodium. J Drug Target. 2003, in press.

5 Fang, J., and Maeda, H. Factors and mechanism of "EPR" effect and the enhanced antitumor effects of macromolecular drugs including SAMNCS. *In:* H. Maeda (ed.). Polymer drugs in clinical stage: advantages and prospects. Kluwer Academic, UK, 2003, in press.

6 Maeda, H., Fang, J., Sawa, T. and Konno, T. Factors and mechanism of EPR effect and clinical outlook of SMANCS. *In:* R. Han (ed.), Cancer Chemotherapy and Chemoprevention. Science Press, Beijing, China, 2003, in press.

7 Maeda, H., Fang, J., Inuzuka, T. and Kitamoto, Y. Vascular permeability enhancement in solid tumor: various factors, mechanisms and implication. Int. Immunopharm. 2003, in press.

8 Fang, J., Sawa, T., Akaike, T., Greish, K., Sahoo, S. K., Hamada, A., and Maeda, H.

In vivo Antitumor Activity of Pegylated Zinc Protoporphyrin Based on Targeted Inhibition of Heme Oxygenase-1 in Solid Tumors. (submitted to Cancer Res.).

9 Fang, J., Sawa, T., Akaike, T., and Maeda, H. Oxidation Antitumor Therapy via Targeted Delivery of Pegylated D- amino Acid Oxidase Combined with Pegylated Zinc Protoprophyrin . (to be submitted to J Natl. Cancer Inst.).

ACKNOWLEDGEMENTS

I wish to express my deepest gratitude to Professor Hiroshi Maeda of Department of Microbiology, Kumamoto University School of Medicine, for his kind supervision, tireless guidance, invaluable advises, support and encouragement throughout the whole period of my Ph.D. training course, which enabled me to study and research in the field of targeted cancer therapy, and resulted in a fruitful worthy theme of research that I hope would contribute to the further clinical challenge to cure cancer.

I am also greatly indebted to Dr. Takaaki Akaike and Dr. Tomohiro Sawa of Department of Microbiology, Kumamoto University School of Medicine very much, for their intellectual insights, remarkable instructions and wise supervision in pursuing my research.

Special thanks to Dr. Yoichi Miyamoto and all other members in Department of Microbiology, Kumamoto University School of Medicine, for their kindly suggestion, warm help and cooperation.

I also thank Dr. Akinobu Hamada at the Faculty of Pharmacy, Kumamoto University, for helpful discussion about pharmacokinetic analysis in this study.

Finally, I would like to thank the Ministry of Education, Science, Sports and Culture of Japan and the members of Faculty of Kumamoto University School of Medicine for giving me an opportunity to study in Japan.

TABLE OF ABBREVIATIONS

DAO	D-amino acid oxidase
ROS	reactive oxygen species
PEG	polyethylene glycol
XO	xanthine oxidase
EPR effect	enhanced permeability and retention effect
TNBS	trinitrobenzenesulfonic acid
GO	glucose oxidase
TBARS	thiobarbituric acid-reactive substance
AUC	area under the concentration versus time curve
CL	total body clearance
LC_{50}	median lethal concentration
ZnPP	zinc protoporphyrin IX
HO	heme oxygenase
TUNEL	terminal deoxynucleotide transferase (TdT)-mediated dUTP-biotin nick end-labeling
DCDHF-DA	2',7'-dichlodihydrofluorecin diacetate
MDR	multidrug resistance
Pgp	P-glycoprotein
RT-PCR	reverse transcriptase-polymerase chain reaction
MTT	3-(4,5-dimethylthiazol-2-yl)-2,5-diphenyltetrazolium bromide
FITC	fluorescein isothiocyanate
siRNA	small interfering RNA
RES	reticuloendothelial system

CHAPTER 1 INTRODUCTION

Reactive oxygen species (ROS) are potentially dangerous by-products of cellular metabolism that have direct effect on cell development, growth and survival, on aging, and on the development of cancer (1). They are generated during the production of ATP by aerobic metabolism in mitochondria. The leakage of electrons from mitochondria during the electron-transport steps of ATP production generates the reactive oxygen species, such as superoxide ($O_2^{\cdot}$). Superoxide radicals can lead to the production of hydrogen peroxide (H_2O_2), from which further hydroxyl radicals (•OH) are generated in a reaction that either depends on, or is catalysed by Fe^{2+} or Cu^{2+} ions. Cells have evolved a series of antioxidative systems to handle these dangerous natural by-products. These defense systems include intracellular superoxide dismutases (SODs); enzymes that inactivate H_2O_2 (e.g., catalase and glutathione peroxidase); and enzymes or compounds that contribute to scavenging free radicals (e.g., heme oxygenase-1, HO-1) (Figure 1).

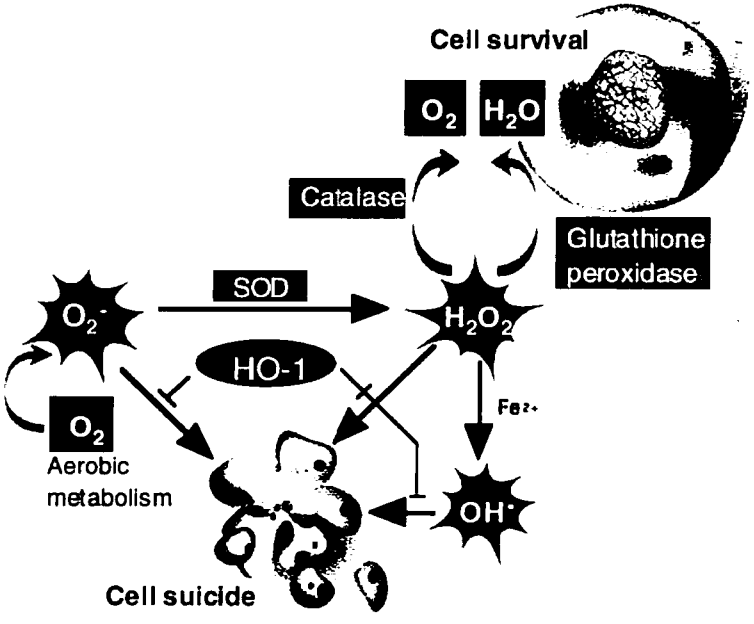

Fig. 1. Reactive oxygen species (ROS) metabolism and the antioxidant defense system in cancer cells. Cancer cells have high levels of metabolism that generate ROS, and the corresponding antioxidative systems (e.g., superoxide dismutase, SOD; heme oxygenase, HO-1) are essential for cancer cells to fight against cytotoxic ROS. Thus, a new antitumor strategy using potentially toxic ROS was challenged, both by directly inducing ROS ($O_2^{\cdot}$, H_2O_2) to tumors, and by targeting these antioxidative enzymes.

ROS are generated by all aerobic organisms and seem to be indispensable for signal transduction pathways that regulate cell growth (2) and reduction-oxidation (redox) status (1). However, overproduction of these highly reactive metabolites can initiate lethal chain reactions that involve oxidation and that damage cellular integrity and survival (1). Hence, ROS have been known to be involved in many diseases, for example, microbial infections, inflammation, ischemia-reperfusion injury, neurologic disorders, Parkinson disease, hypertension, and smoking-related diseases (3, 4). However, on the other hand, tumor cells may also be killed if one can induce the production of cytotoxic ROS to tumor tissues to an adequately high level. Thus, a new concept of cancer chemotherapy can be developed by regulating the redox status in tumor cells, which is named "oxidation therapy" (5-9).

One way to achieve this antitumor therapy is to deliver excess ROS into tumor tissue directly. Among the ROS, H_2O_2 is a good candidate for this therapeutic challenge because of its cytotoxic manner. H_2O_2 readily crosses cellular membranes and causes oxidative damage to DNA (10), proteins (11), and lipids by direct oxidation or via the transition metal-driven Haber-Weiss reaction to the extremely reactive hydroxyl radical (12). It was also reported that H_2O_2 induces apoptosis of a wide range of tumor cells *in vitro* (13-17) via activation of the caspase cascade. Of greater importance, many antitumor agents, such as vinblastine, doxorubicin, camptothecin, and inostamycin, exhibit antitumor activity via H_2O_2-dependent activation of apoptotic cell death, which suggests potential use of H_2O_2 as an antitumor principle (18). However, H_2O_2 is relatively unstable and is a small water-soluble molecule. Those characteristics hamper the utility of H_2O_2 as an antitumor agent that might be selectively delivered to tumor. In fact, H_2O_2 used alone was ineffective when injected into tumor or into the circulation (19-23), perhaps because of its rapid clearance and decomposition by catalase in erythrocytes. Use of an H_2O_2-generating enzyme has been proposed as an alternative approach to developing an H_2O_2-dependent antitumor system. Nathan and Cohn (24) and Ben-Yoseph and Ross (5) reported that glucose oxidase (GO), which generates H_2O_2 during oxidation of glucose, showed antitumor activity in solid tumor models. However, regulation of H_2O_2 production by exogenously administered GO in tumor-bearing hosts is problematic because the availability of its substrates, oxygen and glucose, can not be effectively modulated, with the possible induction of severe systemic side effects because of systemic generation of H_2O_2. In fact, GO

administration to produce H_2O_2 required injection of antioxidants to minimize systemic toxicity (5, 24). In this study, another H_2O_2-generating enzyme, D-amino acid oxide (DAO) was selected, by which the generation of H_2O_2 can be easily modulated because of the scarcity of its natural substrate, D-amino acids, in mammalian organisms (25). Therefore, I anticipated the preferential production of H_2O_2 in tumor, and thus potent antitumor activity of this PEG-DAO system.

On the other hand, many tumor cells seem to have increased rates of metabolism compared with normal cells, which might typically lead to increased production of ROS. In addition, extensive infiltrated leukocytes, e.g., macrophage, have been known to exist in solid tumors as a part of host defense response, which generate ROS against tumor cells. Therefore, the antioxidative systems, e.g., HO-1, catalase, superoxide dismutase (SOD), become much important in tumor for defending against ROS around them. Along similar context, cancer cells may be damaged by inhibiting these antioxidative enzymes. For instance, Huang and colleagues recently found a compound that selectively kill human leukemia cells by inhibiting SOD in tumor cells (9).

In this study, I focused on another important defense enzyme in tumor, HO-1. Heme oxygenase (HO) is the rate-limiting enzyme in the degradation of heme to produce biliverdin, carbon monoxide (CO) and free iron (Fe^{2+}). Biliverdin thus formed is subsequently converted to bilirubin by biliverdin reductase (26, 27). The constitutive isoform of HO (HO-2) is highly expressed in testis and brain under physiological conditions (27). HO-1, an inducible isoform of HO, is found at low levels in most mammalian tissues but is constitutively expressed in liver and spleen (28). Expression of HO-1 is induced by a wide variety of stress-inducing stimuli, including heat shock (29), ultraviolet irradiation (30), hydrogen peroxide (30), heavy metals (30, 31), hypoxia (32), and nitric oxide (NO) (33, 34). Bilirubin has been reported to behave as a potent antioxidant by scavenging free radicals (35-37). CO has also been shown to provide protection of cells against injury of various kinds both *in vitro* and *in vivo* (38, 39).

Because of its protective manner, HO-1 is also indicated in tumor cells to fight against oxidative stresses around them, thus to sustain rapid tumor growth (40). It was previously found the high expression of HO-1, which is relative to that in spleen and liver, in an experimental solid tumor (34). Induction of stresses, e.g., nitric oxide (NO), ischemia, further up-regulated the expression of HO-1 in tumor cells, suggesting that

solid tumor takes advantage of this important enzyme as a protective means for its growth and survival (34). In fact, it was found that tumor growth was remarkably suppressed by administration of a competitive inhibitor of HO-1, zinc protoporphyrin IX (ZnPP) to tumor-bearing rats (34). These findings, thus, indicated a new therapeutic strategy for cancer by use of ZnPP, to target HO-1 in tumors.

To achieve satisfactory antitumor effect by above ROS-generating enzyme and inhibitor of antioxidant enzyme, targeted delivery of them to tumor tissues is indispensable for this antitumor challenge because nonspecific production of ROS may cause oxidative stress-induced side effects in normal organs. Hence, here the concept of the EPR (enhanced permeability and retention) effect (41-54) was utilized. The EPR effect is applicable to macromolecules and lipids in a variety of solid tumors due to the unique characteristics of blood vessels in most solid tumors: (i) ***extensive angiogenesis and hence high vascular density*** (55, 56); (ii) ***extensive extravasation (vascular permeability) induced by various vascular mediators***, such as (a) bradykinin which is produced via the activated kallikrein-kinin system involving proteolytic cascade (52, 54, 57-60), (b) nitric oxide (NO) generated from L-arginine by the inducible form of nitric oxide synthase (iNOS) in leukocytes or in tumor cells (40, 60, 61), (c) vascular permeability factor (VPF)/vascular endothelial growth factor (VEGF) and other cytokines (62-66), (d) prostaglandins involving cyclooxygenases (60, 67), and (e) matrix metalloproteinases (MMPs/collagenases) (68); (iii) ***defective vascular architecture*** (69, 70); (iv) ***impaired lymphatic clearance from the interstitial space of tumor tissues*** (41, 44, 52, 54). In the phenomenon termed EPR effect, biocompatible macromolecules and lipids preferentially and spontaneously leak out of tumor vessels, and remain there as high concentration. This EPR effect is a molecular size-dependent phenomenon, and applicable for the molecular size above 40 kDa (41-46). This dependency exhibits a reverse correlation to the renal clearance of the compounds (41, 52-54). Therefore, EPR effect is observed for any biocompatible macromolecule with a molecular size larger than the renal excretion threshold. EPR effect occurring in solid tumors is a universal phenomenon, which has now become a "gold standard" in the field of drug design for new anticancer drugs (41, 48, 49, 52, 54).

Poly(ethylene glycol) (PEG), one of the best biocompatible polymers, is wildly used for polymeric drug preparation because of its preferred properties such as increased solubility both in organic and aqueous media, increased *in vivo* half-life, and

virtually no toxicity and immunogenicity, nonbiodegradability and ease of excretion from living organisms (71). Thus, it has been used extensively as a covalent modifier of a wide range of proteins/enzymes and drugs, to produce polymer conjugates (72). PEG modified substances become completely different in physicochemical characteristics from nonmodified component, and many pharmacological drawbacks, for example, lack of solubility in water (e.g., native ZnPP) or short plasma half-life and lack of tumor targeting (e.g., native DAO, 39KDa), will be overcome. Furthermore, the modified compound will gain many properties of PEG, i.e., biocompatible macromolecules. As a result, it will show superior pharmacological characteristics for targeted administration. Therefore, in this study, to investigate the *in vivo* effect of ROS on solid tumors, especially their potential for cancer treatment, two polymer conjugates with PEG were prepared: one is H_2O_2-generating enzyme DAO (PEG-DAO), and the other is an inhibitor of antioxidative enzyme HO, ZnPP (PEG-ZnPP). Thus, superior pharmacokinetics and tumor accumulation of these two compounds was anticipated. Consequently, the production of ROS will be induced selectively into tumor, by which kill tumor cells. Furthermore, this therapeutic strategy might be enhanced by combined use of these two compounds.

In this thesis, I will describe the synthesis, pharmacokinetics, antitumor effect, as well as the related mechanisms of PEG-DAO and PEG-ZnPP, in term of their separate or combined roles.

CHAPTER 2 TUMOR-TARGETED DELIVERY OF POLYEHTYLENE GLYCOL-CONJUGATED D-AMINO ACID OXIDASE FOR ANITTUMOR THERAPY VIA ENZYMATIC GENERATION OF HYDROGEN PEROXIDE

2.1 INTRODUCTION

D-Amino acid oxidase (DAO, EC 1.4.3.3) is a flavoprotein that catalyzes the stereoselective oxidative deamination of D-amino acids to the corresponding α-keto acids. During this oxidation reaction, molecular oxygen (O_2) is used as an electron acceptor, and H_2O_2 is generated (73). D-Amino acids do not usually exist in mammalian organisms to a significant level (25). I therefore expected that generation of H_2O_2 could be regulated by modulating exogenous supply of D-amino acids in addition to the delivery of DAO. Thus, it was selected in the present study as the ROS (H_2O_2) generating system.

DAO per se does have a pharmacologic drawback: a short *in vivo* half-life. The molecular size of DAO (39 kDa) is slightly smaller than the renal excretion threshold (~50 kDa), so it would be excreted gradually as previously observed for other small proteins or polymer drugs smaller than 40 kDa (41-46). To overcome this drawback, DAO was chemically modified by conjugation with a biocompatible polymer, PEG. This modification results in an increased in vivo half-life, a reduced antigenicity of the native protein and an inhibition of proteolytic degradation, as reported previously (6, 46, 47, 74).

As described earlier, biocompatible macromolecules accumulate and remain in solid tumor because of the unique characteristics of the tumor vasculature and the impaired lymphatic clearance system. The phenomenon is named EPR effect of macromolecules and lipids in solid tumor (41-54). On the basis of the EPR effect, with DAO conjugated to PEG (PEG-DAO), a high blood level of DAO for a long period and preferential accumulation of DAO in tumor were anticipated. In this study, I describe the synthesis, accumulation in tumor, and antitumor activity of PEG-DAO in a mice model.

2.2 MATERIALS AND METHODS

2.2.1 Materials

DAO (from porcine kidney), D-alanine, and D-proline were purchased from Wako

Pure Chemical Industries, Ltd. (Osaka, Japan). Succinimide-activated PEG (MEC-50HS), with an average molecular size of 5 kDa, was a kind gift from Nippon Oil & Fat Co. (Tokyo, Japan). Other reagents were of reagent grade and were used without further purification.

2.2.2 Animals

Male ddY mice, 6 weeks old and weighing 30-35 g, were from SLC, Inc. (Shizuoka, Japan). All experiments were carried out according to the guidelines of the Laboratory Protocol of Animal Handling, Kumamoto University School of Medicine.

2.2.3 Synthesis and Purification of PEG-DAO

DAO was subjected to gel filtration chromatography to purify the DAO monomer by using Sephadex G-100 (Pharmacia LKB, Uppsala, Sweden). Column size, ϕ20 mm × 50 cm; elution by 50 mM sodium phosphate buffer (pH 7.4); flow rate, 15 ml/h. Under these conditions, DAO monomer was eluted to the 34 to 50 ml fraction (Figure 2), which was collected and condensed to about 1.5 mg/ml protein by use of the Amicon ultrafiltration system (YM-10 membrane; cut-off size Mr 10,000).

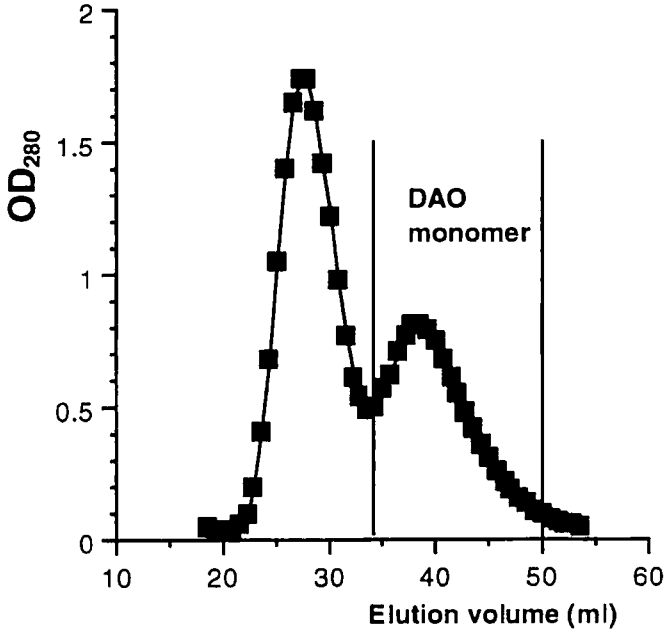

Fig. 2. Size exclusion chromatography of DAO by using Sephadex G-100. The column size was ϕ20 mm × 50 cm, 50 mM sodium phosphate buffer (pH 7.4) was the mobile phase, and the flow rate was 15 ml/h

Succinimidyl PEG was conjugated to the amino group of DAO by using nucleophilic succinimide-activated PEG as described in our previous report (6). In brief, to the DAO solution (1.5-2.0 mg/ml protein in 50 mM sodium phosphate buffer, pH 7.4), succinimide-activated PEG was added at a 3.5 molar excess of PEG per mole of free amino groups in DAO and allowed to react for 1 h at 4°C. The reaction mixture containing PEG-DAO thus obtained was then purified to remove free PEG and other low molecular weight reactants or decomposition products by ultrafiltration with the YM-10 membrane as mentioned above, using 10 times the volume of 0.01 M phosphate-buffered 0.15 M saline (PBS). PEG-DAO was stored in PBS containing 0.1 mM flavin adenine dinucleotide, a cofactor of DAO, at 4°C.

2.2.4 Determination of the Degree of PEG Conjugation

The extent of PEG conjugation with DAO was determined by the method using trinitrobenzenesulfonic acid (TNBS) to measure the decrease in free amino groups (75). Glycine was used as a standard. The protein concentrations of both native DAO and PEG-DAO were quantified by using the DC Protein Assay kit (Bio-Rad Laboratories, Hercules, CA, USA). The molecular size of PEG-DAO thus estimated from the increase relative to PEG was confirmed by approximation via the size exclusion chromatography, described below.

2.2.5 Size Exclusion Chromatography

The preparation described above was further subjected to high-performance liquid chromatography for preparation as well as for analysis. For size exclusion chromatography, the FPLC system (Pharmacia LKB) equipped with a Superose 6 HR 10/30 column (Pharmacia LKB) was used. The mobile phase was 50 mM sodium phosphate buffer (pH 7.4), and monitoring was by absorption at 280 nm.

2.2.6 Enzyme Activity of DAO

Activity of DAO was determined using the horseradish peroxidase-coupled colorimetric assay with *o*-dianisidine as a substrate for horseradish peroxidase. In this assay, the substrate is reduced and color develops with an absorption maximum at 460 nm (76). D-Alanine was used as the substrate at an initial concentration of 0.1 M. The enzyme reaction was carried out at 25°C in 0.1 M Tris-HCl buffer (pH 8.2), where 1 unit of DAO activity is defined as the rate of formation of 1 μmol of H_2O_2 per minute.

2.2.7 *In Vitro* Cytotoxicity Assay

In vitro cytotoxicity of DAO was determined by the 3-(4,5-dimethylthiazol-2-yl)-

2,5-diphenyltetrazolium bromide (MTT) assay (77) with human colon cancer SW480 cells, which were plated in 96-well culture plates (3000 cells/well). Cells were cultured overnight in Dulbecco's modified Eagle's medium with 10% fetal calf serum. SW480 cells were then incubated in the presence of native DAO or PEG-DAO with a substrate (D-proline or D-alanine) for 24-48 h. Toxicity was quantified as the fraction of surviving cells relative to that of untreated controls.

2.2.8 *In Vivo* Distribution of PEG-DAO after i.v. Injection into Tumor-Bearing Mice

Mouse sarcoma S180 cells (2×10^6 cells) were implanted s.c. in the dorsal skin of ddY mice. At 7-10 days after tumor inoculation when tumors reached to a diameter of 5-7 mm but no necrotic areas were apparent, DAO activity in each tissue was measured to quantify the distribution of native DAO and PEG-DAO after i.v. injection. The dose of DAO in both groups was 1.5 units/mouse given via the tail vein. At scheduled time points, from 1 min to 8 h, mice were killed and blood samples were drawn from the inferior vena cava, after which mice were subjected to reperfusion with 10 ml of physiologic saline containing heparin (5 units/ml) to remove blood components in the blood vessels of all tissues. Tumor tissues as well as normal tissues and organs including liver, kidney, spleen, intestine, heart, lung, muscle, and brain were collected and weighed. The enzyme activity of DAO in each tissue was then determined, based on formation of α-keto acid (pyruvic acid) from the reaction between the D-amino acid (D-alanine) and DAO (78).

The pharmacokinetic parameters of native DAO and PEG-DAO were determined by use of a two-compartment model, and the plasma half-life was estimated via the nonlinear least squares program MULTI (79), in which the area under the plasma concentration versus time curve (AUC) was calculated by using the trapezoidal rule and extrapolating to infinity. The total body clearance (CL) was calculated as:

$$CL\ (ml/h) = dose\ (milli\ units)/AUC_{0-\infty}\ (milli\ units \cdot h/ml)$$

2.2.9 *In Vivo* Antitumor Activity of PEG-DAO

Mice with palpable S180 tumors (4-5 mm in diameter) (the tumors implanted as described above) were used to examine the antitumor activity of native DAO and PEG-DAO. Native DAO or PEG-DAO was injected (1.5 units/mouse) i.v., followed by i.p. administration (0.5 mmol/mouse) of D-proline twice daily at 2 and 4 h after native DAO or PEG-DAO injection. Tumor volume was estimated by measuring longitudinal cross

section (L) and transverse section (W) and applying the formula $V = (L \times W^2)/2$.

2.2.10 Thiobarbituric Acid-Reactive Substance (TBARS) Assay

Oxidative cellular damage was determined by assay of lipid peroxide formation via the thiobarbituric acid (TBA) reaction (80). Native DAO or PEG-DAO was injected (1.5 units/mouse) i.v. to mice bearing S180 tumors, after which, 2 and 4 h later, D-proline was administered i.p. (0.5 mmol/mouse). Mice were killed 12 h after the last administration of D-proline. After reperfusion of mice with physiologic saline containing heparin, tumors, livers, and kidneys were collected and weighed followed by homogenization and centrifugation. The TBARS assay was then carried out. The concentration of the product, malondialdehyde, was calculated using extinction coefficient of $1.56 \times 10^5 M^{-1} cm^{-1}$ (81).

2.2.11 Statistical Analysis

All data are expressed as means ± SE. Student's *t* test was used to determine the significance between each experimental group. The difference was considered statistically significant when $P < 0.05$. Same statistical analysis was used the in other studies described in Chapters 3 and 4.

2.3 RESULTS

2.3.1 Synthesis and Characterization of PEG-DAO

Physicochemical and biochemical characteristics of native DAO and PEG-DAO are summarized in Table 1. The reaction resulted in 34.6% modification of the amino groups of DAO with PEG, out of a total of 13 amino groups: 88.7% of the original enzyme activity of native DAO was retained. The molecular size of the PEG-DAO conjugate was estimated to be 63 kDa, according to the degree of loss of amino group by conjugating with PEG as determined by the TNBS assay.

Table 1 Physicochemical and biochemical characteristics of native DAO and PEG-DAO

Type of DAO	Feed ratio[a] (PEG/NH_2)	Free NH_2[b] (% conjugation)	M_r[c] (kDa)	Enzyme activity (U/mg of protein, % of control)
Native DAO	0	13 (0)	39	7.25 (100)
PEG-DAO	3.5	8.5 (34.6)	63	6.43 (88.7)

[a] Molar excess of PEG added over amino groups of the enzyme.
[b] Determined by the TNBS method
[c] Calculated from the loss of amino groups and attached PEG.

The increase in the apparent molecular size of PEG-DAO in aqueous media was confirmed by size exclusion chromatography (Figure 3).

Fig. 3. Size exclusion chromatography of native DAO and PEG-DAO. The column was Pharmacia LKB Superose 6 HR (10 mm inner diameter. 30 cm length); the elution buffer was 50 mM sodium phosphate buffer (pH 7.4); absorbance was detected at 280 nm.

2.3.2 *In Vitro* Cytotoxicity of PEG-DAO

Cytotoxicity of DAO was first examined via an *in vitro* system using colon cancer SW480 cells. D-Proline was used as the substrate because it was reported that D-proline is the optimal substrate for DAO with a high turnover rate (82). PEG-DAO alone and D-proline alone showed no cytotoxicity against SW480 cells (data not shown). In contrast, PEG-DAO showed remarkable concentration-dependent cytotoxicity in the presence of D-proline (Figure 4). This toxicity was completely nullified by the addition of catalase (Figure 4A), indicating that H_2O_2 plays a critical role in the observed cytotoxicity induced by the PEG-DAO/D-proline system. Similar results were obtained by using native DAO plus D-proline (data not shown). In addition, with the same concentration of PEG-DAO (10 mU/ml). D-proline showed much greater

cytotoxic activity (median lethal concentration [LC_{50}] of 0.3 mM) than did D-alanine (LC_{50} of 3.6 mM) (Figure 4B).

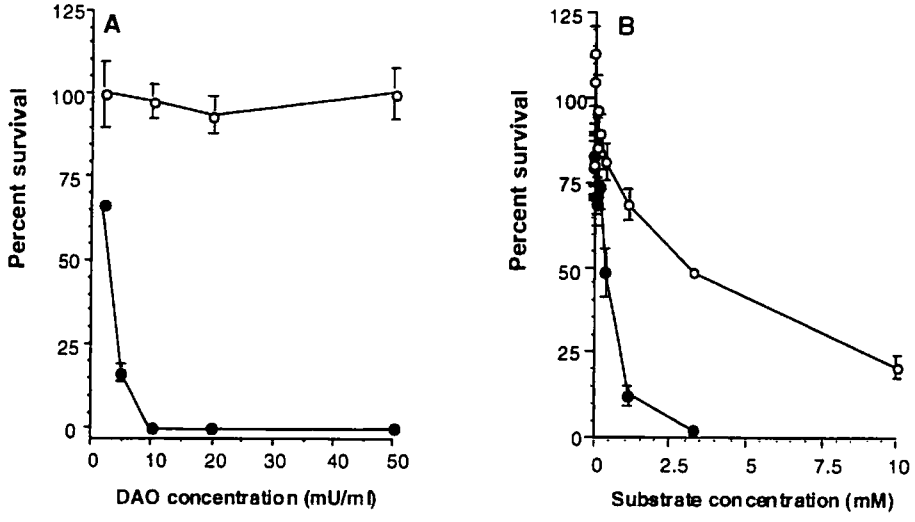

Fig. 4. ***In vitro*** **cytotoxicity of PEG-DAO.** A, Cultured SW480 cells were exposed to increasing amounts of PEG-conjugated DAO in the presence of 50 mM D-proline for 24 h in the absence (●) or presence (○) of catalase (1000 units/ml). B, SW480 cells were incubated with 10 mU/ml PEG-DAO in the presence of D-alanine (○) or D-proline (●) for 48 h. Cell viability was determined by means of the MTT assay. Values were represented as means ± SE (n = 6).

2.3.3 *In vivo* Distribution of PEG-DAO after i.v. Injection

After i.v. injection, native DAO was rapidly cleared from the circulation, with a plasma half-life of 14 min. Whereas, PEG conjugation significantly prolonged the half-life to 36 min based on the enzyme activity (Table 2, Figure 5). The AUC value of PEG-DAO was approximately 2.9 times higher than that of native DAO, whereas urinary clearance of PEG-DAO conjugate decreased to about one third of that of native DAO (Table 2). As shown in Figure 6A, a significant level of endogenous DAO activity was detected in kidney and liver, which is consistent with a previous report (78). Four hours after administration of native DAO, the enzyme activity in plasma and tumor increased slightly (Figure 6). However, PEG conjugation dramatically improved intratumor accumulation of DAO as well as plasma level of DAO after i.v. injection (Figure 6), i.e., 3.2-fold higher enzyme activity relative to native DAO and 7.4-fold to untreated control (background) in tumor: 2.4-fold relative to native DAO and

9.1-fold to untreated control in plasma. It is noteworthy that PEG-DAO administration showed no effect on the enzyme activity in normal organs and tissues including liver, kidney, spleen, intestine, heart, lung, muscle, and brain (Figure 6). These findings suggest that tumor-targeted delivery of DAO can be achieved with relatively high efficiency by pegylating DAO.

Table 2 Pharmacokinetic parameters of native DAO and PEG-DAO

Material	$t_{1/2}$ (min)[a]	$AUC_{0-\infty}$ [(mU•h/ml)][b]	CL (ml/h)[c]
Native DAO	14	1100	1.36
PEG-DAO	36	3147	0.48

[a] Half-life ($t_{1/2}$) required to reach to half-concentration of time zero by interpolation.
[b] Area under the plasma concentration versus time curve.
[c] Total body clearance.

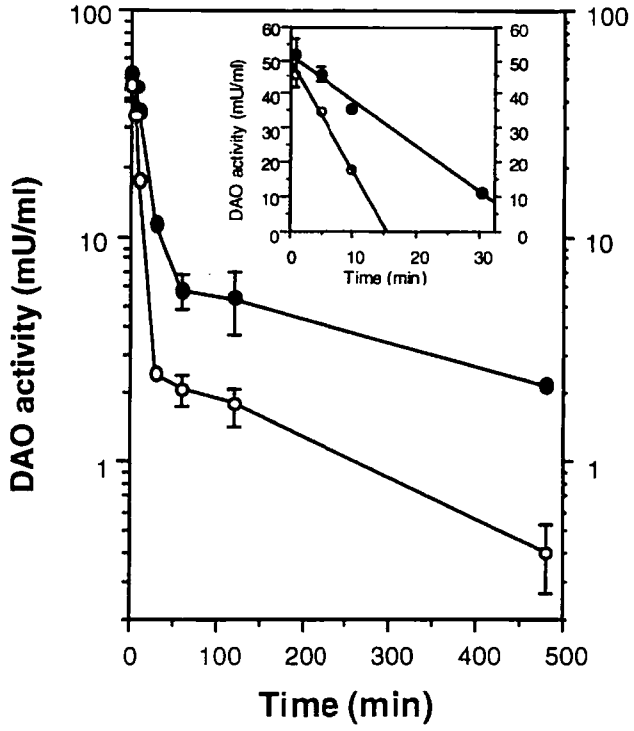

Fig. 5. Enzyme activity in plasma after i.v. injection of native DAO or PEG-DAO. Native DAO (○) or PEG-DAO (●) (each at 1.5 units/mouse) was injected i.v. into S180 tumor-bearing ddY mice. After scheduled periods, mice were killed and plasma was collected. Enzyme activity in the plasma was quantified by measuring pyruvic acid formation after addition of D-alanine. See text for details. Results are expressed as means ± SE (n = 3 - 6). The inset shows the linear change in enzyme activity in plasma within 30 min after i.v. injection of native DAO or PEG-DAO.

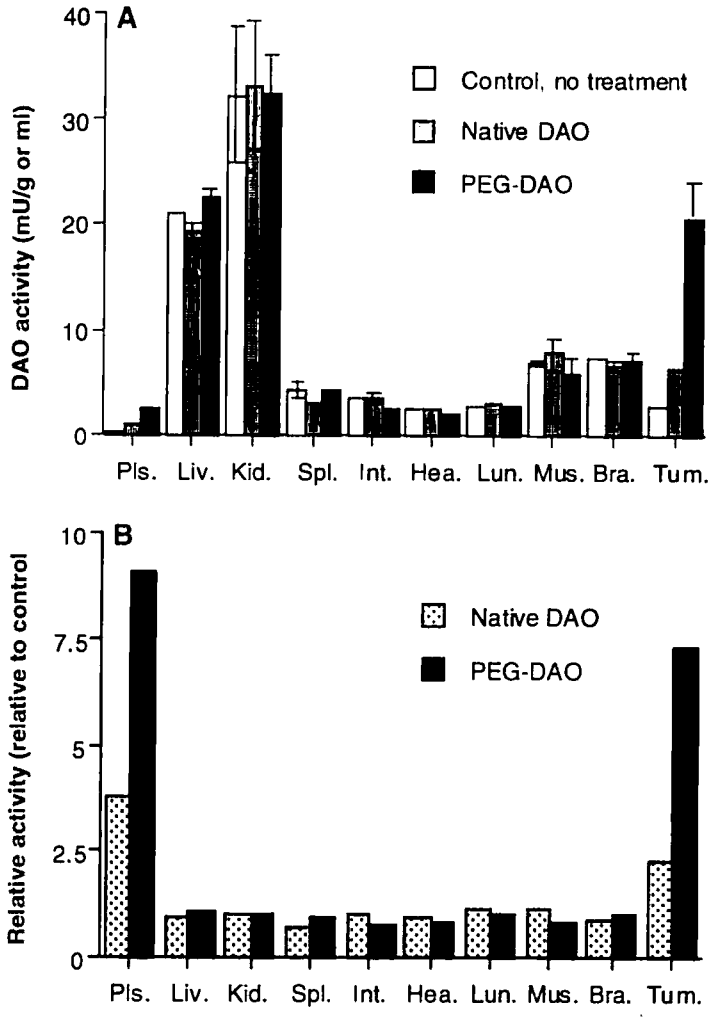

Fig. 6. Body distribution of native DAO and PEG-DAO in tumor-bearing mice. Native DAO or PEG-DAO (each at 1.5 units/mouse) was administrated i.v. After 4 h, mice were killed and DAO activity in each tissue was measured as described in Figure 3. A shows DAO activity in various organs and tumor tissue. B shows the ratio of activity of native DAO or PEG-DAO versus activity in untreated mice. Results are expressed as means ± SE (n = 3 - 6). Abbreviations, Pls., plasma; Liv., Liver; Kid., Kidney; Spl., spleen; Int., intestine; Hea., heart; Lun., lung; Mus., Muscle; Bra., brain; Tum., tumor.

2.3.4 *In Vivo* Antitumor Activity of PEG-DAO

Native DAO or PEG-DAO was administrated i.v., and after an adequate lag time (e.g., 2 or 4 h after each administration) to allow the accumulation of DAO in the tumor (see Figure 4), the substrate D-proline was administered by i.p. injection. This treatment procedure allows generation of cytotoxic H_2O_2, predominantly at the tumor site.

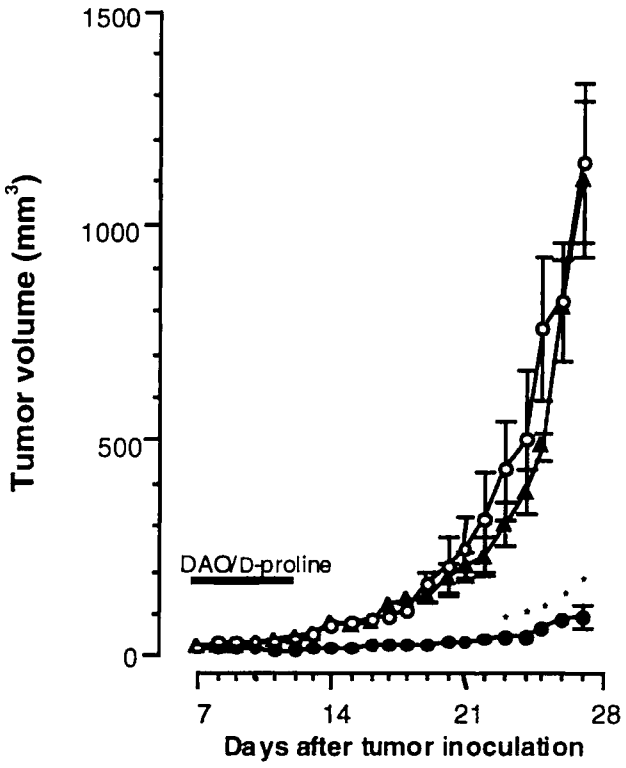

Fig. 7. Antitumor effect of PEG-DAO in the S180 solid tumor model. S180 cells (2×10^6 cells) were implanted s.c. in ddY mice. Seven days after inoculation, mice were treated with 1.5 units of native DAO (▲) or PEG-DAO (●) followed by D-proline (0.5 mmol, i.p., 2 and 4 h after DAO administration). The open circle indicates the result for control mice (no treatment). Data are means (n = 4 - 8); bars indicate SE, $*P < 0.001$ (PEG-DAO group versus control group and native DAO group). See text for details.

As shown in Figure 7, tumor growth was significantly suppressed in mice administered PEG-DAO plus D-proline. Growth suppression continued to at least 27 days after tumor implantation, which was 15 days after the last treatment with PEG-DAO and D-proline. In contrast, no significant antitumor effect was observed in mice treated with native DAO plus D-proline. The average tumor weights on the 27th day after tumor inoculation for the groups treated with PEG-DAO/D-proline and native DAO/D-proline and the control were 0.34 ± 0.11, 1.5 ± 0.15, and 1.59 ± 0.32 g, respectively (mean±SE, $P < 0.001$; control versus PEG-DAO/D-proline group). In separate experiments, neither PEG-DAO nor D-proline alone showed any antitumor activity (data not shown).

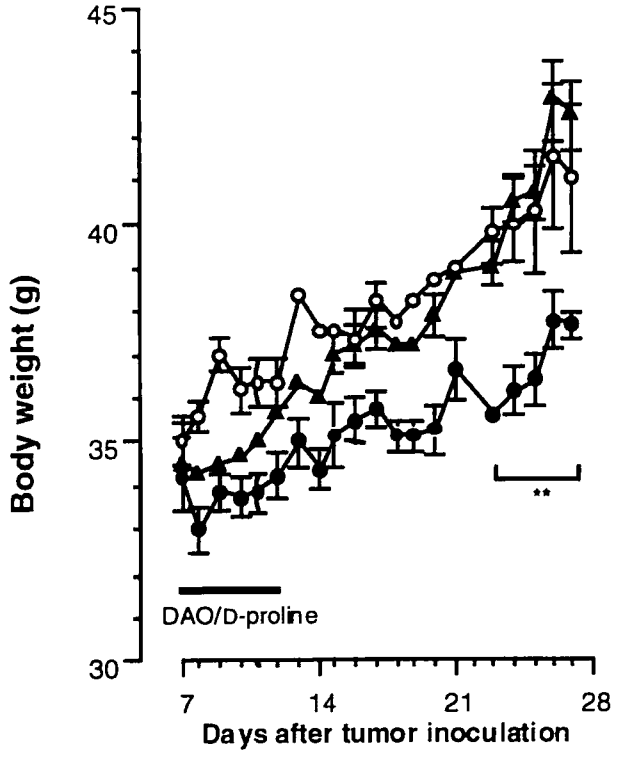

Fig. 8. Body weight changes in ddY mice treated with native DAO or PEG-DAO. The treatment protocol is the same as that described in Figure 7. ○, control mice without any drug; ●, PEG-DAO plus D-proline: ▲, native DAO plus D-proline. Data are means ± SE (n = 3 or 4), $^{**}P < 0.01$ (PEG-DAO group versus control group and native DAO group).

Figure 8 shows body weight changes in mice receiving different treatments. At the early stage of observation, especially during the first 5 days of treatment, a slight loss of body weight, in both PEG-DAO/D-proline group and native DAO/D-proline group (there were no significant difference in body weight between these two groups), was observed compared with the control group (given no drugs). After the cessation of treatment, body weight of both groups increased gradually at a rate of growth comparable to that of the control mice. At later stage of observation, a significant difference in body weight was found between PEG-DAO/D-proline group versus native DAO/D-proline group and the control group ($P < 0.01$), however, it is mostly attributed to the difference of tumor weight between them.

2.3.5 Tumor-Specific Oxidative Damage caused by PEG-DAO plus D-proline

Administration of PEG-DAO plus D-proline caused a significant increase in TBARS, a marker of oxidative cellular injury, in tumor tissue (Figure 9A). In contrast,

no significant increase in TBARS production was observed either in the control group (given no drugs) or in the native DAO treatment group. Also, PEG-DAO/D-proline treatment did not affect the level of TBARS in the liver and kidney where intrinsic DAO activity with or without PEG-DAO treatment was high (Figure 6). This finding suggests that PEG-DAO/D-proline treatment generates cytotoxic H_2O_2 selectively at the tumor site rather than in normal tissues. PEG-DAO had a greater effect on TBARS in the tumor tissue than did native DAO (Figure 9B)

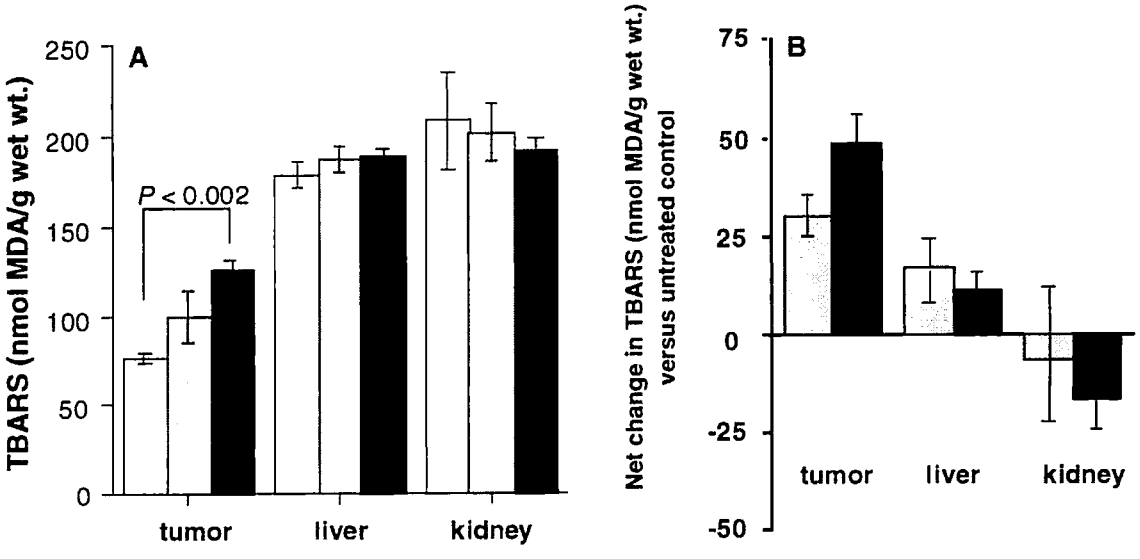

Fig. 9. TBARS in tumor tissue, liver, and kidney of tumor-bearing ddY mice after treatment with native DAO or PEG-DAO. D-Proline was administered (0.5 mmol/mouse) at 2 and 4 h after DAO injection (1.5 units/mouse). Twelve hours after the last D-proline administration, mice were killed; tumor tissue, liver, and kidney were collected and then were subjected to the TBARS assay. A, Malondialdehyde (MDA) production in tumor, liver and kidney. B, Net production of malondialdehyde in each tissue. Results are expressed as means ± SE (n = 3 - 6). □, control (no treatment); ■, native DAO plus D-proline; ■, PEG-DAO plus D-proline.

2.4 SUMMARY

I report here that administration of two nontoxic components, PEG-DAO followed after adequate lag times by D-proline resulted in remarkable tumor regression. Because of the EPR effect, tumor-targeted delivery of PEG-DAO became thus possible, and subsequent injection of D-proline selectively generated potent cytotoxic compound H_2O_2 preferentially at the tumor site. Consequently, effective antitumor activity by H_2O_2 can be accomplished without any apparent toxicity to normal tissues and organs.

CHAPTER 3 *IN VIVO* ANTITUMOR ACTIVITY OF PEGYLATED ZINC PROTOPORPHYRIN BASED ON TARGETED INHIBITION OF HEME OXYGENASE-1 IN SOLID TUMOR

3.1 INTRODUCTION

HO-1 is suggested to serve as a key biological molecule in the adaptation to and/or defense against oxidative stress and cellular stress. It is interesting to note that several tumors, including renal cell carcinoma (83) and prostate tumors (84) in humans, express a high level of HO-1. The high HO-1 expression was also found in experimental solid tumors, i.e., the rat hepatoma AH136B (34) and the mouse sarcoma S180. This level of HO-1 expression was relative to that in spleen and liver (85). In these models, inducible NO synthase (iNOS) was also up-regulated, and thus tumor tissues were exposed to oxidative stress related to NO and/or its reactive metabolites (40, 60). Administration of the HO inhibitor zinc protoporphyrin (ZnPP), via tumor-feeding artery significantly suppressed the growth of AH136B tumors, which suggests a vital role for HO-1 in tumor growth (34). These findings also indicate a potentially beneficial role of HO inhibitors as novel anticancer agents. However, the *in vivo* antitumor activity of HO inhibitors developed so far has not yet been fully proved.

Metalloporphyrins constitute a class of compounds in which the central iron of heme is replaced by various other metals such as cobalt, zinc, manganese, chromium, or tin (86). These metalloporphyrins function as competitive inhibitors of the HO reaction because of their inefficient binding to molecular oxygen, which prevents HO from degrading the metalloporphyrins (86). Although these metalloporphyrins may exhibit antitumor activity, as has been shown for ZnPP, their very low solubility in water limits further investigation of these compounds *in vivo*. To overcome this limitation, a water-soluble derivative of ZnPP was recently developed by conjugating it with a water-soluble polymer, PEG (85). This polymer conjugate PEG-ZnPP, similar to native ZnPP, remained active as an HO inhibitor (85). Furthermore, i.v. injection of PEG-ZnPP significantly reduced intratumor HO activity. In addition to the issue of solubility, PEG-ZnPP formed multimolecular associations with molecular size larger than 70 KDa in aqueous media (85). Therefore, by virtue of EPR effect, I anticipated a high blood level of PEG-ZnPP for a long period and preferential accumulation of PEG-ZnPP selectively in tumor site. Consequently, superior antitumor effect by taking

advantage of the tumor selective inhibition of HO-1 activity in tumor was expected. In the present study, *in vivo* antitumor activity of PEG-ZnPP was demonstrated by using a murine solid tumor model. Pharmacokinetics and side effects due to PEG-ZnPP treatment were also examined.

3.2 MATERIALS AND METHODS

3.2.1 Materials

Protoporphyrin IX was purchased from Sigma Chemical Co. (St. Louis, MO, USA). The succinimidyl derivative of PEG (MEC-50HS), which reacts with a primary amino group (71), with an average molecular weight of 5000, was kindly provided by NOF Co., Tokyo, Japan. Other reagents were of reagent grade and were used without further purification.

3.2.2 Animals

Male ddY mice, 6 weeks old and each weighing 30-35 g, were from SLC, Inc. (Shizuoka, Japan). All experiments were carried out according to the guidelines of the Laboratory Protocol of Animal Handling, Kumamoto University School of Medicine.

3.2.3 Synthesis of PEG-ZnPP

The synthesis, purification, and characterization of PEG-ZnPP were described in our previous work (85). The scheme of PEG-ZnPP preparation is shown in Figure 10.

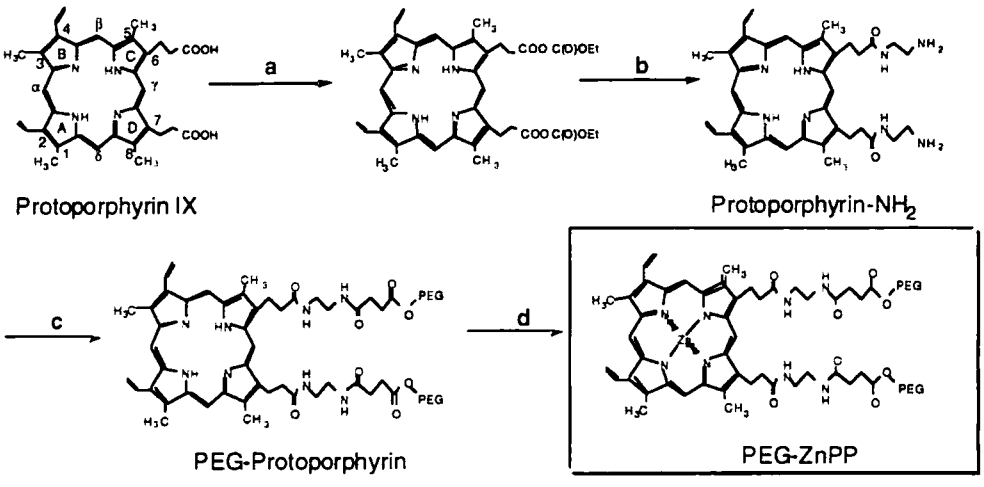

Fig. 10. Scheme of PEG-ZnPP synthesis. Reagent a), ethylchloroformate and Triethylamine in tetrahydrofuran (THF); reagent b), ethylenediamine in THF; reagent c), polyethylene glycol (PEG) in CH_3Cl; reagent d), zinc acetate in CH_3Cl.

3.2.4 Cell Culture

Human colon cancer SW480 cells were cultured in Dulbecco's modified Eagle's medium with 10% fetal calf serum at 37°C in a 5% CO_2-95% air atmosphere.

3.2.5 RT-PCR Assay for Expression of HO-1 in SW480 cells

Total RNA from SW480 cells were isolated using TRIzol reagent (Life Technologies. Inc.. Grand Island. NY. USA). according to the manufacturer's instruction. The RT-PCR reaction was performed by use of the method of Abraham (87).

3.2.6 Induction of Intracellular ROS by PEG-ZnPP

SW480 cells were seeded in 12-well plates (10^5 cells/well). After an overnight preincubation. cells were treated by PEG-ZnPP for 8 h. Then, 10 μM (final concentration) of 2',7'-dichlodihydrofluorescein diacetate (DCDHF-DA) was added, and the cells were cultured for an additional 30 min. The esterified form of DCDHF-DA can permeate cell membranes and then be deacetylated by intracellular esterases. The resultant compound, dichlorodihydrofluorescein (DCDHF) being remained in cells. reacts with ROS to give a fluorescent compound, dichlorofluorescein (DCF) (88). The amount of intracellular ROS was quantitated as a function of fluorescence intensity measured by flow cytometry (BD FACSCalibur 3A. San Jose. CA, USA).

3.2.7 MTT Assay

In vitro cytotoxicity was determined by the 3-(4.5-dimethylthiazol-2-yl)-2.5-diphenyltetrazolium bromide (MTT) assay (77). Cells were seeded in 96-well plates (3000 cells/well), and after an overnight preincubation, cells were exposed to indicated concentrations of PEG-ZnPP for 48 h. The toxicity was quantified as the fraction of cells surviving relative to untreated controls.

3.2.8 *In Vitro* Apoptosis Assay

Pro-apoptotic activity of PEG-ZnPP was determined by a flow cytometric assay with Annexin V-FITC (89), by using the Annexin V-FITC Apoptosis Detection Kit (BD PharMingen, San Diego, CA. USA). In brief, the cells that plated in 12-well plates (10^5 cells/well) were preincubated overnight. Then. cells were treated by PEG-ZnPP for 24 h. After the cells were harvested by use of a rubber policeman, they were subjected to Annexin V-FITC kit and propidium Iodide (PI). The number of apoptotic cells was quantified by flow cytometry.

To study the effect of HO inhibition on induction of apoptosis. HO-1 expression

was specifically suppressed by using a 21-nucleotide duplex small interfering RNA (siRNA) (90), which targets nucleotides 612-630 of the HO-1 mRNA coding sequence. The sequences of ribonucleotides used were 5'-rGACUGCGUUCCUGCUCAACdTdT-3' and 5'-GUUGAGCAGGAACGCAGUCdTdT-3' (Dharmacon Research Inc., Lafayette, CO, USA). SW480 cells (10^5 cells/well) were plated in 6-well plates and were preincubated overnight, after which 2 μg of siRNA was introduced into the cells by use of TransMessenger Transfection Reagent according to the manufacturer's directions (QIAGEN GmbH, Hilden, Germany). Forty-eight hours after transfection, cells were harvested and subjected to the apoptosis assay described above.

3.2.9 Pharmacokinetics of PEG-ZnPP after i.v. injection

In vivo pharmacokinetics of native and PEG-ZnPP were examined by use of ^{65}Zn-labeled derivatives and were compared with that of native, nonpegylated ZnPP. Radiolabeled PEG-ZnPP was prepared by the same method as that described in ref. 84, in which ^{65}Zn-labeled Zinc acetate (PerkinElmer Japan Co. Ltd., Yokohama, Japan) was used. Radiolabeled native ZnPP was obtained by chelating ^{65}Zn to protoporphyrin IX in dimethyl sulfate. Free ^{65}Zn (as zinc acetate) in PEG-ZnPP and native ZnPP was removed by gel chromatography with a Sephadex G-25 column (PD-10 columns, Amersham Pharmacia Biotech AB, Uppsala, Sweden) and dialysis against distilled water, respectively. Mouse sarcoma S180 cells (2×10^6 cells) were implanted s.c. in the dorsal skin of ddY mice. The study of the body distribution of PEG-ZnPP was performed on days 7-10 after tumor inoculation, when tumors were 5-7 mm in diameter but without necrotic region.

Mice received i.v. injection of ^{65}Zn-labeled PEG-ZnPP via the tail vein (15,000 cpm (2.3 kBq)/mouse, 0.1 ml/mouse). After scheduled time periods, mice were killed and blood samples were drawn from the inferior vena cava, and mice were then subjected to reperfusion with 10 ml of saline containing heparin (5 units/ml) to remove blood components in blood vessels of the tissues. Tumor tissues as well as normal tissues, including liver, spleen, kidney, intestine, heart, lung, brain, and muscle, were collected and weighed. Radioactivity of these tissues was measured by using gamma counter (Wallac 1480 WIZARD™ 3", Pharmacia Biotech, Truku, Finland).

3.2.10 *In Vivo* Antitumor Activity of PEG-ZnPP

Another group of ddY mice, implanted with S180 tumor cells as just described, was used to examine the therapeutic efficacy of PEG-ZnPP. Tumor-bearing mice were

treated with the reagents of interest at 7 days after tumor inoculation, when tumors had achieved a diameter of 4-5 mm. PEG-ZnPP (1 or 3 mM, 0.1 ml) was administered (equivalent to 1.5 or 5 mg ZnPP/kg, i.v., expressed as 1.5 or 5 mg/kg in the rest parts) daily for 6 days. In control experiments, mice received physiological saline (0.1 ml) instead of the PEG-ZnPP solution. The tumor volume and body weight of the mice were measured daily during the period of investigation. Values for the tumor volume (V) were determined by measuring the longitudinal cross section (L) and the transverse section (W) and then applying the formula $V = (L \times W^2)/2$.

3.2.11 Measurement of HO Activity

Tumor, spleen, and liver tissues from mice with or without PEG-ZnPP treatment were homogenized with a Polytron homogenizer in ice-cold homogenate buffer containing protease inhibitors (20 mM potassium phosphate buffer, pH 7.4, plus 0.25 M sucrose, 2 mM EDTA, 2 mM phenylmethylsulforyl fluoride, and 10 μg/ml leupeptin). Homogenates were centrifuged at 10,000 *g* for 30 min at 4°C, after which the resultant supernatant was ultracentrifuged at 105,000 *g* for 1 h at 4°C. The microsomal fraction obtained in pellet was suspended in 0.1 M potassium phosphate buffer, pH 7.4, followed by sonication for 2 s at 4°C. The reaction mixture that was used for measurement of HO activity was composed of microsomal protein (1 mg), cytosolic fraction of rat liver (1 mg of protein) as a source of biliverdin reductase, 33 μM hemin, and 333 μM NADPH of 1 ml of 90 mM potassium phosphate buffer, pH 7.4. The mixture was incubated for 15 min at 37°C, at which point the reaction was terminated by addition of 33 μl of 0.01 M HCl. The bilirubin formed in the reaction was extracted with 1 ml of chloroform, and the bilirubin concentration was determined spectroscopically by measuring the difference in absorbance between 465 and 530 nm (Δ OD = $OD_{465} - OD_{530}$), with a molar extinction coefficient of 40 mM^{-1} cm^{-1}.

3.2.12 Western Blotting for Expression of HO-1

The microsomal fraction obtained by ultracentrifugation as just described was used for HO-1 analysis. Total microsomal protein (25 μg each sample) in tissue homogenates was separated by electrophoresis with sodium dodecyl sulfate (%0.1)-polyacrylamide (12%) gels, and was transferred to Immobilon polyvinylidene difluoride membranes (Millipore Co., Ltd., Bedford, MA, USA). This process was followed by reaction with a 5000-time diluted polyclonal antibody to HO-1 (OSA-150, Victoria, BC,

Canada) overnight at 4°C. Subsequently, the membranes were treated by a horseradish peroxide linked anti-rabbit IgG with a dilution of 1000-time (Amersham International plc, Buck, UK) for additional 1 h. The protein band that reacted immunologically with the antibodies was visualized by using the ECL system (Amersham), combined with chemiluminescence detection with Hyperfilm (Amersham).

3.2.13 Determination of Blood Count and Blood Chemistry

Mice bearing S180 tumors about 5-7 mm in diameter were used for this study. Twenty-four hours after PEG-ZnPP treatment as described above, mice were killed and blood samples were obtained from the inferior vena cava. RBC and WBC counts and hemoglobin (Hb) level were determined by routine clinical laboratory techniques (91). Plasma obtained by centrifugation was used for measurement of alanine aminotransferase (ALT), aspartate aminotransferase (AST), blood urea nitrogen (BUN) and creatinine (Cr).

3.2.14 *In Situ* Apoptosis Detection

As described earlier, tumor, liver, and kidney were collected after reperfusion of the mice with 10 ml of physiologic saline containing heparin (5 units/ml), and were used for the apoptosis assay and for the histological examination that is discussed below. *In vivo* induction of apoptosis by PEG-ZnPP treatment was detected by using the terminal deoxynucleotide transferase (TdT)-mediated dUTP-biotin nick end-labeling (TUNEL) method (92), with an *in situ* apoptosis detection kit (TACS; Trevigen Inc., Gaithersburg, MD, USA), according to the manufacturer's instruction. Tissue specimens from the mice were embedded in an embedding dishes (Greiner bio-one Co., Ltd., Tokyo, Japan) using Tissue-Tek™ O.C.T. Compound (Sakura Finetechnical Co., Ltd., Tokyo, Japan) and were stored at –80°C before use. Cryosections (10 μm thick) were prepared for this assay. Serial sections were used for the TUNEL assay. TUNEL-positive cells were counted in four different fields per sample, and counts were expressed per square millimeter of tissue section.

3.2.15 Histological Examination

Some tissue specimens collected as described above, were fixed with 10% buffered neutral formalin solution and were then embedded in paraffin. Sections were stained with hematoxylin-eosin (H&E staining).

3.3 RESULTS

3.3.1 *In Vitro* Cytotoxicity of PEG-ZnPP as Related to Increased Oxidative Stress

SW480 cells cultured *in vitro* did express HO-1 mRNA, as demonstrated by RT-PCR (Figure 11A). As shown in Figure 11B, PEG-ZnPP, at concentrations of 5.4 to 54 μM, exhibited a cytotoxic effect in a dose-dependent manner. This cytotoxic effect was largely reversed by addition of the antioxidant, *N*-acetylcysteine (NAC), which suggests involvement of increased oxidative stress in the cytotoxic action of PEG-ZnPP. In addition, PEG conjugated protoporphyrin IX (PEG-PP), a metal-free analogue of PEG-ZnPP that does not inhibit HO, had no cytotoxic effect at the same concentration range (Figure 11B).

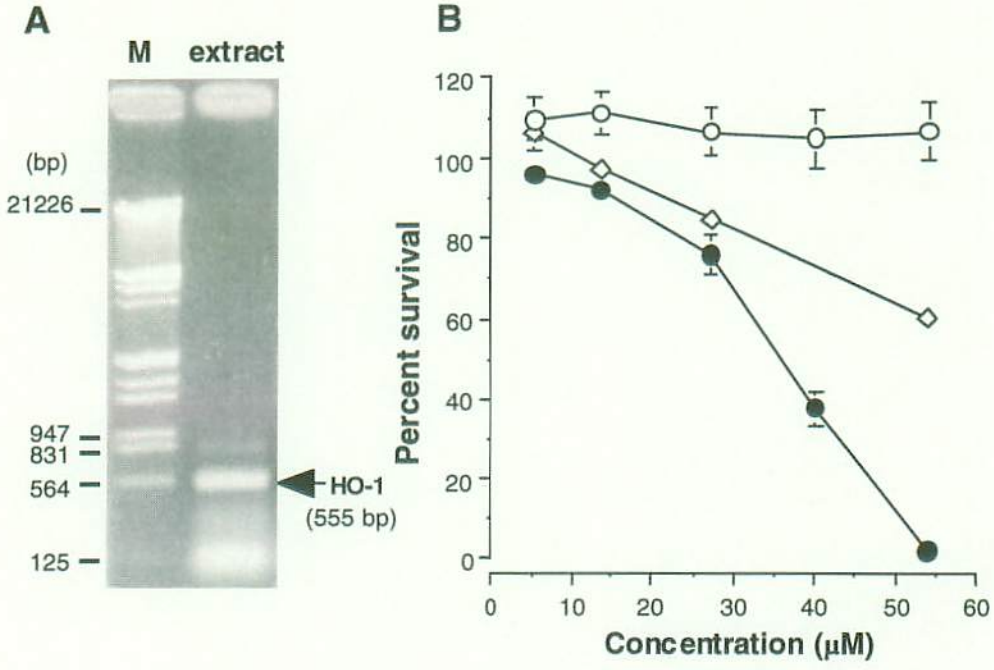

Fig. 11. ***In vitro*** **cytotoxicity of PEG-ZnPP.** A. RT-PCR detection of HO-1 mRNA expressed in SW480 cells. M, Molecular size markers; extract, total RNA extracted from SW480 cells. B. Cytotoxicity of PEG-ZnPP. SW480 cells were exposed to increasing concentrations of PEG-ZnPP or PEG-PP for 48 h. Other SW480 cells were incubated with PEG-ZnPP in the presence of *N*-acetylcysteine (2 mM). Cell viability was then determined by means of the MTT assay. ●, PEG-ZnPP; ○, PEG-PP; ◇, PEG-ZnPP plus NAC. Values are means ± SE (n = 6 wells).

To investigate whether PEG-ZnPP increases intracellular production of ROS in SW480 cells, flow cytometry was performed with the use of oxidant-sensitive fluorescence probe, DCDHF (88). As shown in Figure 12, PEG-ZnPP increased

fluorescence intensity of cells in a dose-dependent manner, whereas PEG-PP did not. These findings suggest that increased oxidative stress is due to inhibition of HO activity.

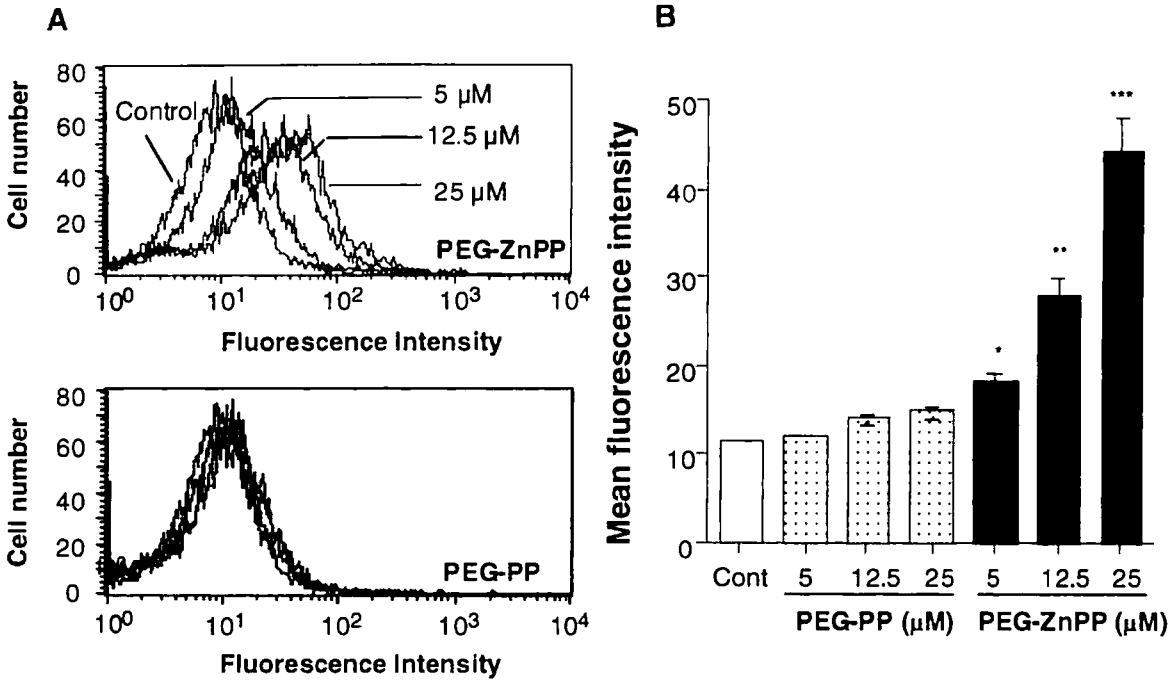

Fig. 12. Induction of intracellular ROS production in SW480 cells by treatment with PEG-ZnPP. SW480 cells were treated with increasing concentrations of PEG-ZnPP or PEG-PP for 8 h. The amount of intracellular ROS was measured by flow cytometry. Values are means ± SE (n = 3 wells). $^{*}P < 0.01$, $^{**}P < 0.005$, $^{***}P < 0.002$, PEG-ZnPP versus control.

3.3.2 PEG-ZnPP Inducted Apoptosis in SW480 Cells

To investigate whether apoptosis is involved in the cytotoxic action of PEG-ZnPP, a fluorescein-labeled Annexin V assay was performed to detect the apoptotic SW480 cells after PEG-ZnPP treatment. PEG-ZnPP induced apoptosis in these cells in a concentration-dependent manner (Figure 13A). This result correlated well with the increase in formation of intracellular oxidant, as shown in Figure 12B. Targeted knockdown of HO-1 expression by siRNA induced apoptosis of cultured SW480 cells (Figure 13B). This finding indicates that HO-1 plays an important role in preventing apoptosis of SW480 cells under the study conditions. Thus, PEG-ZnPP-induced inhibition of HO activity results in apoptosis through a mechanism involving the increased oxidative stress.

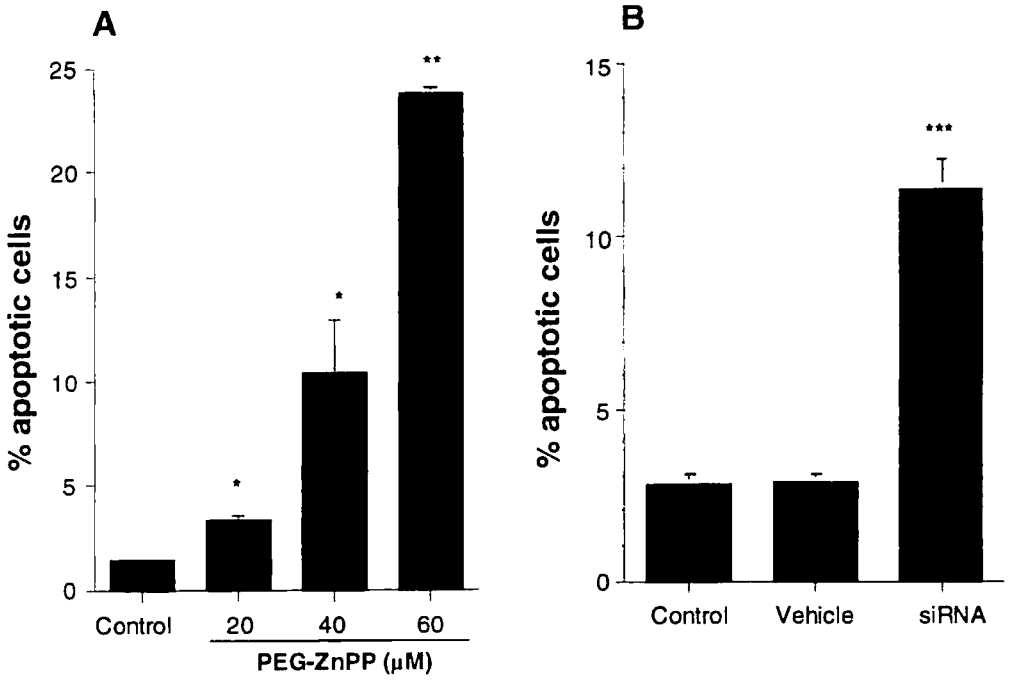

Fig. 13. Induction of apoptosis in SW480 cells by PEG-ZnPP. Cells were treated with increasing concentrations of PEG-ZnPP for 24 h (A) or with siRNA for 48 h (B). The number of apoptotic cells was determined by flow cytometry, and the percentage of apoptotic cells (per the total number of calculated cells) is shown. Values are means ± SE (n = 3 wells). In (A), $*P < 0.05$, $**P < 0.00001$ versus control. In (B), vehicle indicates the result for cells treated with TransMessenger Transfection Reagent only (without siRNA); siRNA indicates the result for cells transfected with siRNA for HO-1 mRNA; $***P < 0.0007$.

3.3.3 Pharmacokinetics of PEG-ZnPP after i.v. Injection

As shown in Figure 14A, nonpegylated native ZnPP rapidly disappeared from the blood circulation after i.v. injection; the area under the concentration versus time curve (AUC) was 2,505 ± 396 (cpm • h)/ml. In contrast, PEG-ZnPP showed a significantly longer circulation time. An AUC value that was more than 40 times higher (102,290 ± 11,649 (cpm • h)/ml) was achieved by PEG-ZnPP.

It is important to note that in tumor tissue PEG-ZnPP accumulates in a time-dependent manner, with a maximum increase at 48 h, whereas native ZnPP reached a maximum accumulation at 8 h after administration and then gradually disappeared (Figure 14B).

Body distribution analysis showed a PEG-ZnPP buildup in the liver and the spleen, both of which have an active reticuloendothelial system (RES) (93). This observation

suggests that PEG-ZnPP after systemic administration is trapped by the RES. Besides liver and spleen, tumor tissue showed a PEG-ZnPP accumulation greater than that in other normal tissues (Figure 14C), which suggests a preferential concentration of PEG-ZnPP in tumor.

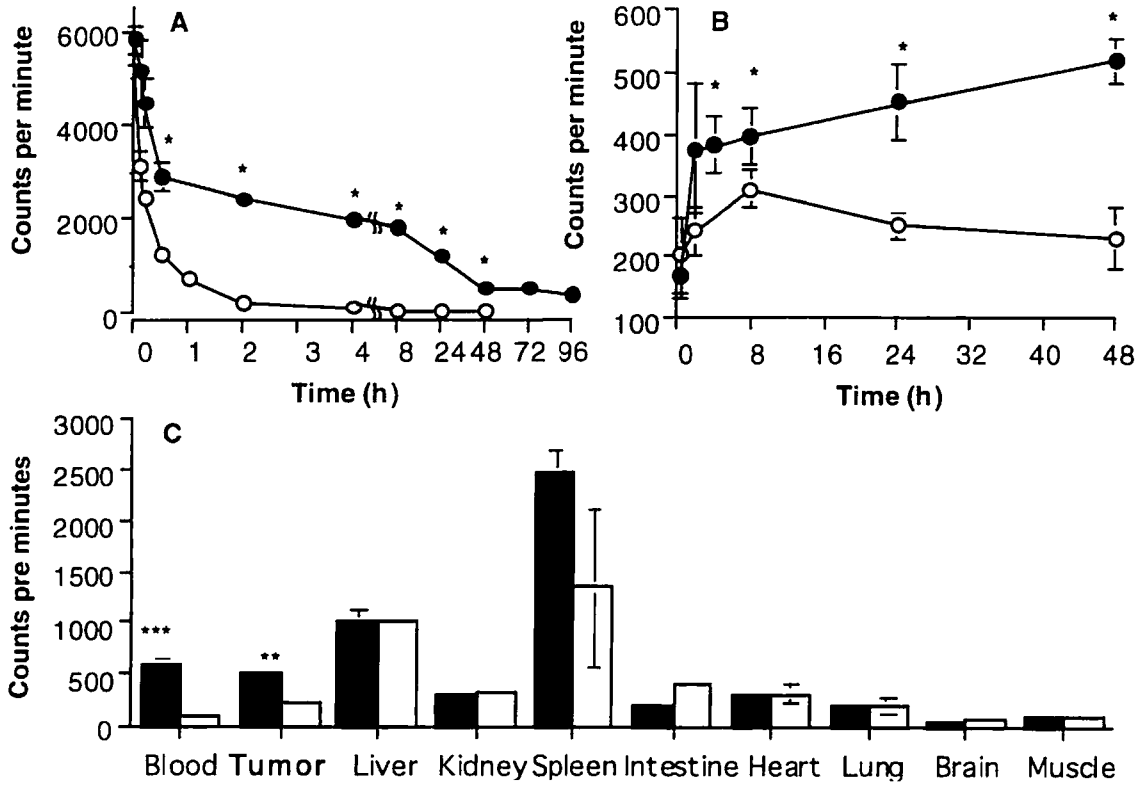

Fig. 14. Pharmacokinetics of PEG-ZnPP and native ZnPP in ddY mice bearing S180 tumor as determined by using radioactive derivatives. Radiolabeled native ZnPP or PEG-ZnPP was injected i.v. into tumor-bearing mice. After scheduled time periods, mice were killed and samples of blood, tumor, and normal tissues and organs were collected. Radioactivity of each tissue or organ was then measured. (A) Plasma level of PEG-ZnPP (●) and native ZnPP (○). (B) Tumor accumulation of PEG-ZnPP (●) and native ZnPP (○). (C) Body distribution of native ZnPP (open bars) and PEG-ZnPP (filled bars) 48 h after i.v. injection. Results (A, B, C) are expressed as means ± SE (n = 3 or 4). *P < 0.01, **P < 0.005, *** P< 0.0005, PEG-ZnPP versus native ZnPP.

3.3.4 *In Vivo* Antitumor Activity of PEG-ZnPP

As shown in Figure 15, tumor growth was significantly suppressed in mice receiving PEG-ZnPP treatment. With the dose of 5 mg/kg, tumor growth was continuously suppressed until at least 36 days after tumor implantation, which was 24

days after the last administration of PEG-ZnPP. Complete regression of tumor growth was observed in two of eight tumors after treatment with PEG-ZnPP (5 mg/kg). In contrast, in mice treated with PEG-PP tumor growth was delayed. In addition, the effect of native ZnPP was not examined in this *in vivo* study because it is not soluble in water at the dose mentioned above, which is not suitable for systemic administration. The average tumor weights on the 36th day after tumor implantation for the groups treated with the high dose of PEG-ZnPP (5 mg/kg), the low dose of PEG-ZnPP (1.5 mg/kg) or PEG-PP and for the untreated control were 1.43 ± 0.36, 2.17 ± 0.39, 7.04 ± 0.98, and 6.14 ± 1.03 g, respectively.

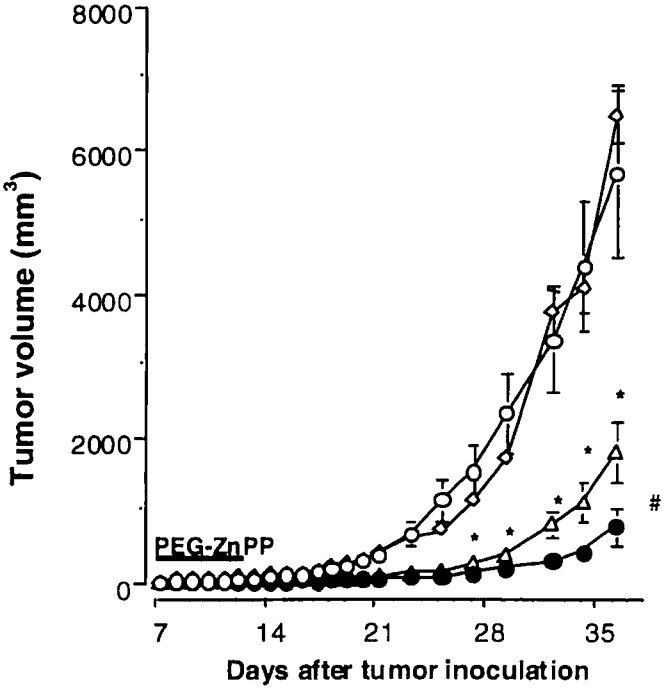

Fig. 15. Antitumor effect of PEG-ZnPP in the S180 solid tumor model. S180 cells (2 × 10^6 cells) were implanted subcutaneously in ddY mice. Seven days later, mice were treated with different doses of PEG-ZnPP (●, 5 mg/kg: △, 1.5 mg/kg) or PEG-PP (◇, 5 mg/kg) daily for 6 days. Control mice (○) received injections of physiological saline. Data are means ± SE (n = 6-8). *P < 0.001. PEG-ZnPP treatment groups versus PEG-PP treatment and control groups. #, Complete regression of tumor growth was observed in two of eight tumors after treatment with PEG-ZnPP (5mg/kg).

3.3.5 Body Weight Changes after PEG-ZnPP Treatment

Figure 16 shows body weight changes of mice receiving different treatments.

Early in the observation periods, no group showed a loss of body weight. During the later stage of investigation, however, a significant difference in body weight was observed in the groups treated with PEG-ZnPP compared with the nontreated control group and the PEG-PP treated group ($P < 0.05$). This body weight change is attributed primarily to the difference in tumor weight among these groups as mentioned above.

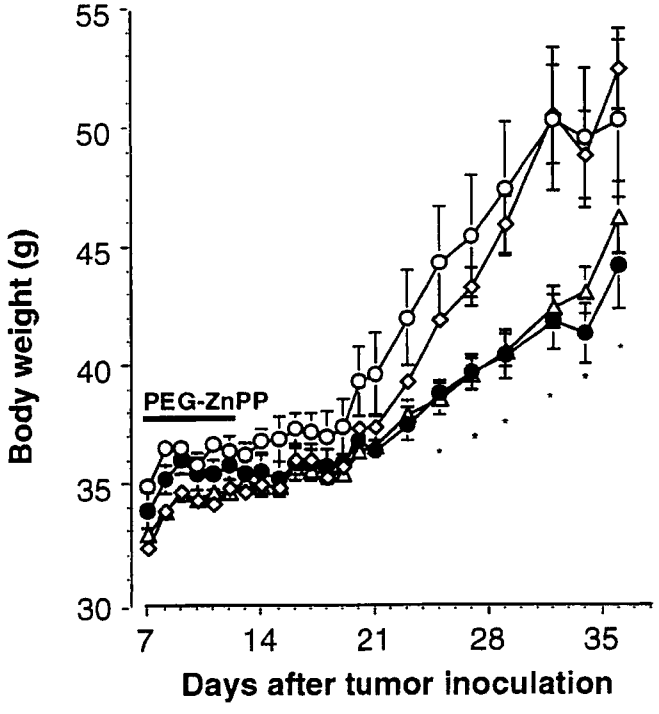

Fig. 16. Body weight changes of ddY mice treated with PEG-ZnPP. The treatment protocol was the same as that described for Fig. 15. ○, control mice bearing S180 tumor, no treatment; ●, 5 mg/kg PEG-ZnPP; △, 1.5 mg/kg PEG-ZnPP; ◇, 5 mg/kg PEG-PP. The body weight change of mice without tumor was similar to that of group ● and ◇ (not shown). Data are means ± SE (n = 3 or 4). *$P < 0.05$ for group ● and △ compared with control and PEG-PP groups.

3.3.6 *In Vivo* Induction of Tumor Cell Apoptosis of PEG-ZnPP

The TUNEL assay was used to examine apoptosis induced *in vivo* by PEG-ZnPP. Untreated control and PEG-PP treated specimens showed only a negligible TUNEL-positive staining, whereas strong TUNEL-positive staining was observed for PEG-ZnPP-treated S180 tumor tissue (Figure 17A). Morphometric analysis of TUNEL-positive cells in the S180 solid tumors showed that the numbers of positive cells in the control group, the PEG-PP-treated group, and the 5 mg/kg PEG-ZnPP-treated group

were 25.9 ± 5.7, 55.5 ± 14.9, and 560.5 ± 77.3/mm^2, (Figure 17B).

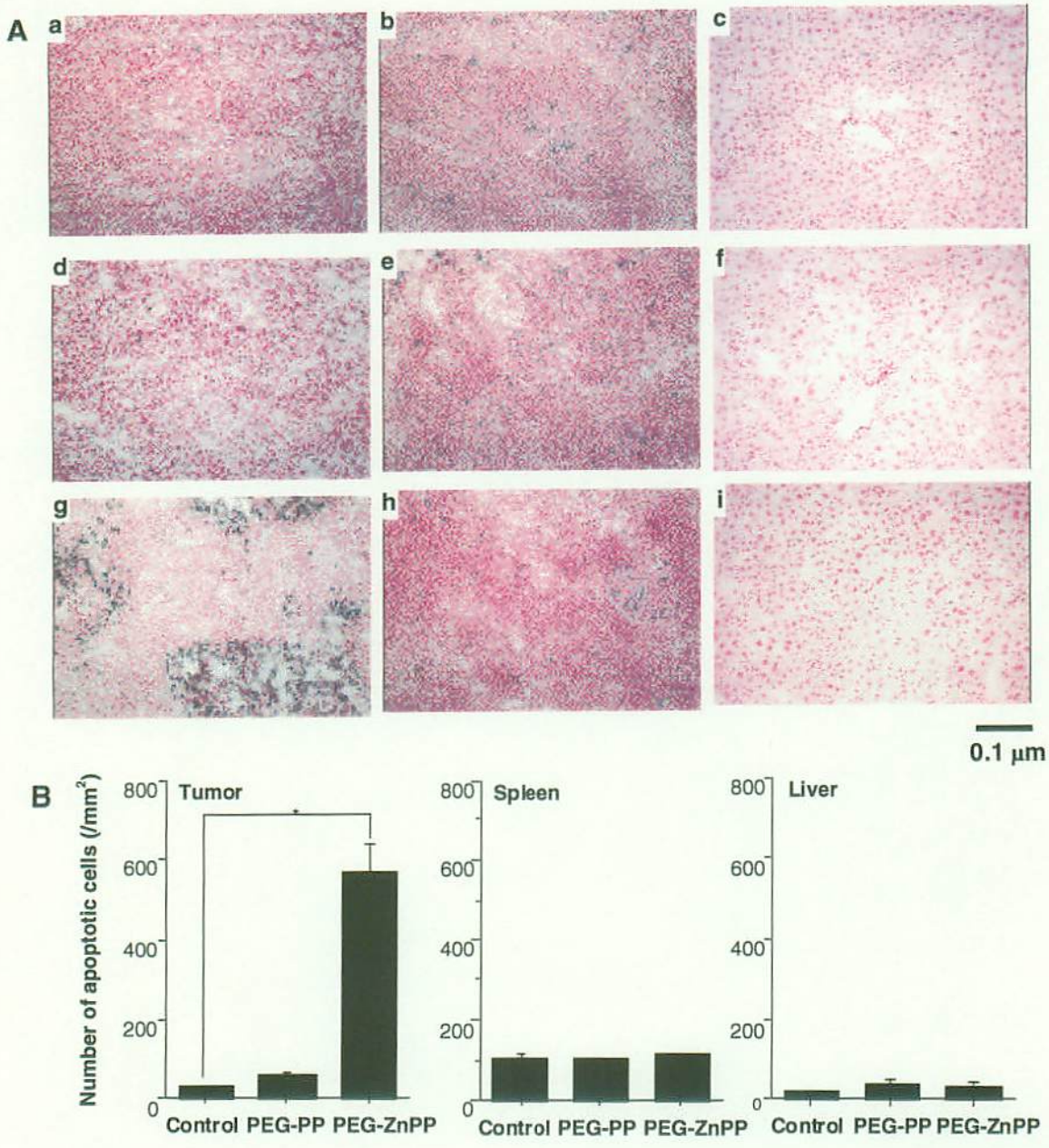

Fig. 17. Induction of apoptosis in S180 solid tumors by PEG-ZnPP. Each specimen was collected and examined 24 h after treatment. The treatment protocol was the same as that described for Fig. 15. (A) TUNEL staining for each group: a, d, g, tumor; b, e, h, spleen; c, f, i, liver. a, b, c, untreated control; d, e, f, PEG-PP; g, h, i, PEG-ZnPP. Apoptosis exhibits a dark blue staining. Morphometric analyses of the number of TUNEL-positive cells in each specimen are shown in (B). TUNEL-positive cells were counted in four different fields per sample, and counts were calculated as the number of positive cells per mm^2. Data are means ± SE (n = 3 for each group). *P < 0.005, PEG-ZnPP group versus control and PEG-PP groups.

In contrast, no significant increase in apoptosis was found after PEG-ZnPP treatment in liver and spleen (Figure 17).

3.3.7 Targeted Inhibition by PEG-ZnPP of HO Activity in S180 Solid Tumor

To clarify whether the induction of apoptosis *in vivo*, and thus the suppression of tumor growth caused by PEG-ZnPP were due to the inhibition of HO activity, the protein expression and activity of HO-1 in tumor and spleen after PEG-ZnPP treatment were examined. As shown in Figure 18A, HO-1 protein was clearly expressed in tumor and spleen of ddY mice. More important, even though HO-1 protein increased in tumor after PEG-ZnPP treatment (Figure 18A), this treatment was significantly inhibited (by ~50%) HO activity in the tumor (Figure 18B). In contrast, PEG-ZnPP treatment neither increased HO-1 protein nor inhibited HO activity in the spleen (Figure 18, spleen). Similarly, HO activity in liver was not affected by PEG-ZnPP treatment (data not shown).

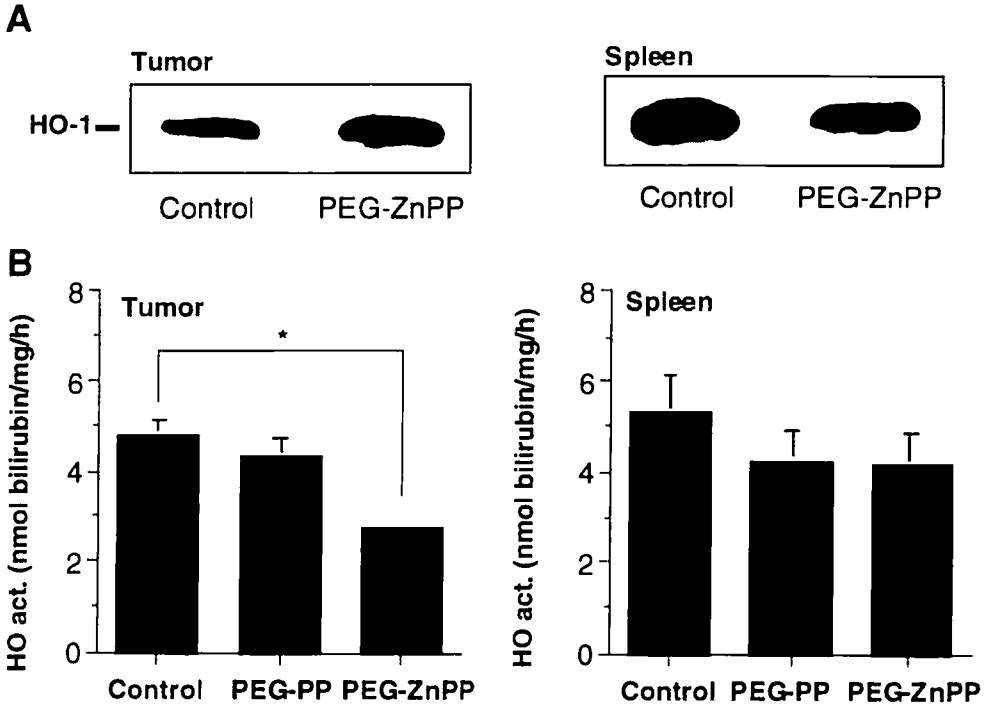

Fig. 18. Modulation by PEG-ZnPP of HO-1 expression (A) and activity (B) in the S180 solid tumor model. Tumor-bearing ddY mice were treated with PEG-ZnPP according to the same protocol as that described for Fig. 15. Twenty-four hours after the last injection, tumors and spleens were obtained and were used for (A) Western blotting of HO-1 protein and (B) HO activity after PEG-ZnPP treatment. Values are means ± SE (n = 4). *P < 0.005 PEG-ZnPP versus PEG-PP and control (P < 0.03, PEG-ZnPP group versus PEG-PP group).

3.3.8 Evaluation of Side Effects in PEG-ZnPP Treatment

Because of a report that ZnPP is potentially toxic to both myeloid and erythroid cell growth (94), the hematological toxicity of PEG-ZnPP treatment was investigated in S180 tumor-bearing mice treated by means of blood cell measures (RBC, WBC, Hb). No significant decreases in RBC and WBC counts and Hb level were found after PEG-ZnPP treatment at the dose effective against cancer, compared with the measures in the untreated control (Table 3). In addition, no significant effects of PEG-ZnPP treatment were seen in biochemical assays of major organs (liver, kidney), i.e., plasma ALT, AST, LDH, BUN, Cr values (Table 3).

Table 3 Changes in RBC, WBC, hemoglobin and plasma enzyme levels 24 h after PEG-ZnPP treatment of ddY mice [a]

	RBC (10^4/μl)	WBC (/μl)	Hb (g/l)	BUN (mg/dl)
Control	1074 ± 106.0	8013 ± 862	133.0 ± 13.4	19.7 ± 1.1
PEG-PP (5 mg/kg)	1056 ± 50.5	7063 ± 1154	121.3 ± 5.8	17.6 ± 1.8
PEG-ZnPP (5 mg/kg)	1066 ± 29.8	7983 ± 2902	131.5 ± 7.4	18.2 ± 1.3

	Cr (mg/dl)	AST (IU/l/at 37°C)	ALT (IU/l/at 37°C)	LDH (IU/l/at 37°C)
Control	0.09 ± 0	249 ± 79.5	37.0 ± 4.4	7611 ± 3221
PEG-PP (5 mg/kg)	0.10 ± 0	221 ± 21.6	40.5 ± 5.5	4754 ± 567
PEG-ZnPP (5 mg/kg)	0.11 ± 0.01	181 ± 29.7	28.5 ± 1.4	4833 ± 1078

[a] No significant difference was found between each treatment group and the control group in all the selected indices.
Values are presented as means ± SE.

3.3.9 Histological Examination

Tumor tissues showed necrotic changes, whereas no pathological changes were observed in liver and spleen, after PEG-ZnPP treatment (data not shown).

3.4 SUMMARY

I demonstrate here that tumor-targeted inhibition of HO activity could be achieved by using the water-soluble HO inhibitor PEG-ZnPP. Inhibition of intratumor HO

activity leads to apoptosis of tumor cells by, at least in part, decreasing the bilirubin level, which results in sensitizing tumor cells to oxidative stress (see Figure 19). This finding suggests that PEG-ZnPP may intensify the antitumor activity of other chemotherapeutics that can produce reactive oxidants and that it may act selectively in tumor tissue because of the EPR effect. Many chemotherapeutics including conventional antitumor agents such as doxorubicin and camptothecin (18), as well as PEG-conjugated oxidoreductases such as PEG-xanthine oxidase (6) and PEG-D-amino acid oxidase (see Chapter 2), are known to generate ROS and exhibit antitumor effects. The effect of PEG-ZnPP discussed here is consistent with this antitumor strategy. In addition, with regard to the molecular mechanism related to the action of PEG-ZnPP, there may be other possibilities than enhancing ROS production, which will be discussed in Chapter 5.

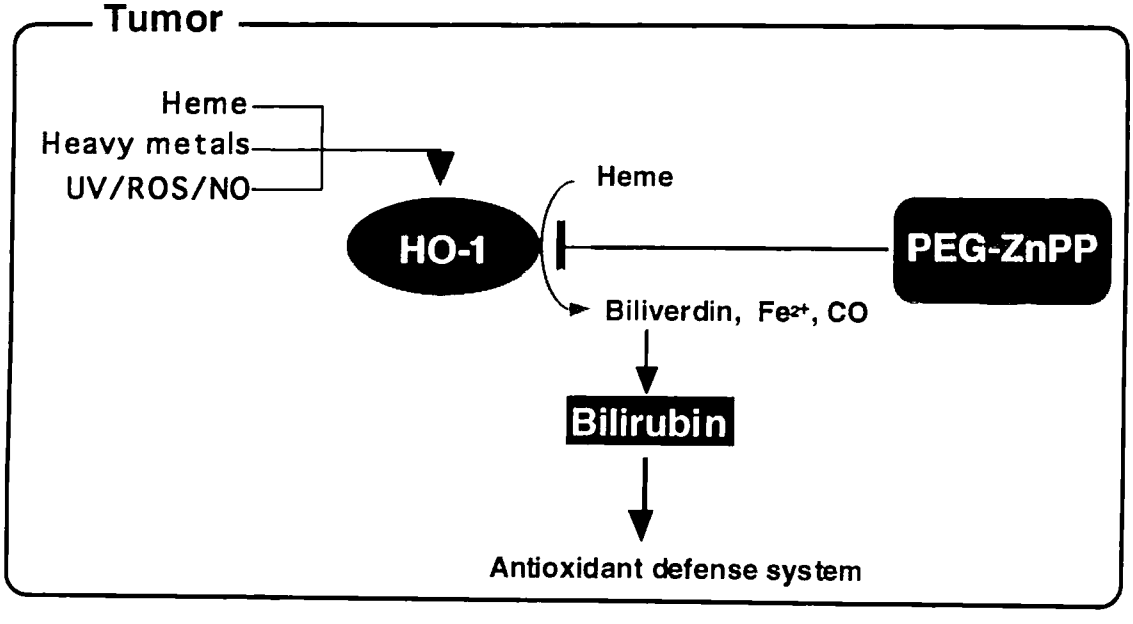

Fig. 19. Mechanism of PEG-ZnPP Induced Antitumor Effect by Inhibition of HO-1 in Tumor. Decreased activity of HO-1 by PEG-ZnPP's inhibition leads to, at least partially, increased susceptibility of tumor cells to ROS derived from various sources, such as macrophage and NADPH oxidase and xanthine oxidase of damaged tissues of the host. Consequently, tumor cells were killed, at least partially by cytotoxic ROS via an apoptosis pathway.

CHAPTER 4 OXIDATION ANTITUMOR THERAPY VIA TARGETED DELIVERY OF PEGYLATED D- AMINO ACID OXIDASE COMBINED WITH PEGYLATED ZINC PROTOPORPHYRIN

4.1 INTRODUCTION

As mentioned earlier, oxidation antitumor therapy represents a new strategy of cancer chemotherapy by increasing the oxidative burden of tumor cells (5-9). Along this line, a series of new antitumor agents have been developed, including PEG-DAO or PEG-ZnPP, which enhanced ROS production in solid tumor either exogenously (PEG-DAO) or endogenously (PEG-ZnPP). Consequently, remarkable antitumor activities of these two compounds were achieved separately in a murine tumor model, as described in Chapters 2 and 3.

Combination of two or more anticancer drugs is popular and has been verified effective in both basic cancer researches and clinical anticancer challenges, which can reduce the side effect of each single agent and, in many cases, dramatically enhance the antitumor effect via the synergistic effect of different drugs. Thus, a more effective antitumor therapy was anticipated by tumor-targeted delivery of PEG-DAO system combined with PEG-ZnPP. This chapter describes synergistic antitumor activity of these two compounds, in term of *in vitro* and *in vivo* aspects.

4.2 MATERIALS AND METHODS

PEG-DAO and PEG-ZnPP were prepared as described in Chapters 2 and 3. In *in vitro* experiments, human colon cancer SW480 cells were used for intracellular ROS, cytotoxicity (MTT) and apoptosis assay, after treated by H_2O_2 and PEG-ZnPP (see Chapter 3 for detail). H_2O_2 was used instead of PEG-DAO system because it is the effective product of this system.

In *in vivo* experiments, ddY mice bearing mouse sacroma 180 cells were used as tumor model. Six days after tumor inoculation when tumors reached to a diameter of 4-5 mm but no necrotic areas were apparent, the antitumor activity of PEG-DAO and/or PEG-ZnPP was examined. Twenty-four hours after PEG-ZnPP administration (1.5 mg /kg, i.v.), PEG-DAO was injected daily (0.75 units/mouse) i.v. for continuous 3 days, followed by i.p. administration (0.5 mmol/mouse) of D-proline 4 h after PEG-DAO injection, after which D-proline was injected daily (0.5 mmol/mouse) for additional two

days. Tumor volume and body weight of the mice were measured daily during the period of investigation. Meanwhile, 24 h after treatment, mice were killed and blood, tumor, and important organs, e.g., liver, kidney, and lung, were collected for blood count and blood biochemistry, *in situ* apoptosis TUNEL assay (tumor) and histological examination (tumor, liver, kidney and lung). These protocols are described in Chapter 3 in detail.

4.3 RESULTS

4.3.1 Induction of Intracellular ROS Generation by H_2O_2/PEG-ZnPP Treatment

To investigate whether the synergistic effect is operative by this combination treatment on intracellular production of ROS , a flow cytometry method was performed by using the oxidant-sensitive fluorescence probe DCDHF as described in Chapter 3. As shown in Figure 20, a moderate increase of intracellular ROS generation was found either by H_2O_2 (500 μM) or by PEG-ZnPP (5 μM) treatment alone, whereas a significant increase of ROS, more than the sum of H_2O_2 and PEG-ZnPP individually, was found in this combination treatment. These findings suggest the synergistic effect of these two agents. Similar results were found by using PEG-DAO instead of H_2O_2 (data not shown).

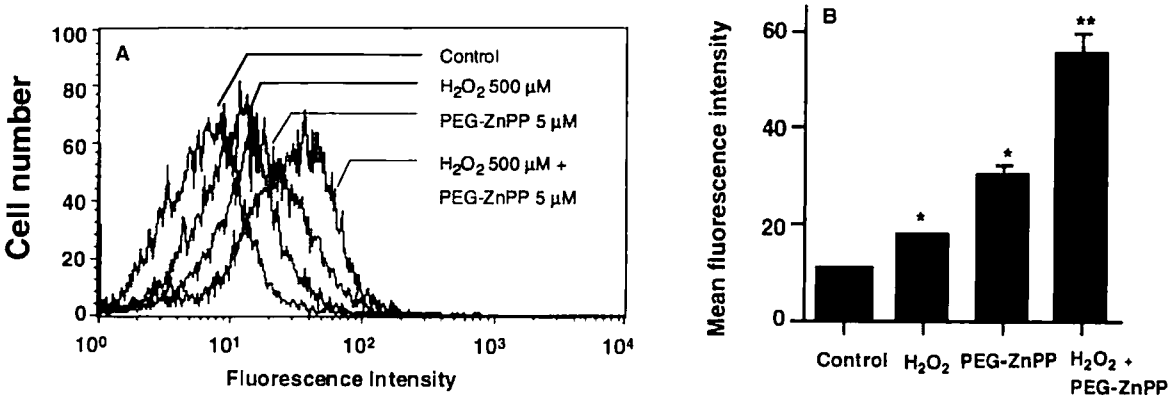

Fig. 20. Induction of intracellular ROS production in SW480 cells by H_2O_2 or PEG-ZnPP alone or in combination. SW480 cells were treated with 500 μM H_2O_2 and/or 5 μM PEG-ZnPP for 8 h. The amount of intracellular ROS was measured by flow cytometry. Values are means ± SE (n = 3). *$P < 0.005$, **$P < 0.001$, versus control.

4.3.2 Enhanced *In Vitro* Cytotoxicity of ROS or ROS-generating anticancer drugs by PEG- ZnPP

To further verify the synergistic effect of this combination treatment, a MTT assay was performed to investigate the cytotoxicity of various ROS (H_2O_2 for Figure 21A: *t*-butyl hydroperoxide (*t*-BOOH) for 21B) and ROS-generating anticancer drugs (Camptothecin for Figure 21C: Doxorubicin for 21D; see ref. 18) combined with PEG-ZnPP. PEG-ZnPP (5 μM) alone showed no cytotoxicity against SW480 cells (Figure 11B). However, it significantly enhanced the cytotoxicity of H_2O_2, e.g., at the concentration of 200 μM, H_2O_2 alone resulted in a cell death of 10.9% in total cells, whereas combination treatment with PEG-ZnPP resulted in a cell death of 29.3% in total cells (Figure 21A). Under the same conditions, enhanced cytotoxic effects by PEG-ZnPP were also observed with *t*-BOOH, camptothecin and doxorubicin (Figure 21B, C, D). Similar result was also obtained for PEG-DAO (data not shown).

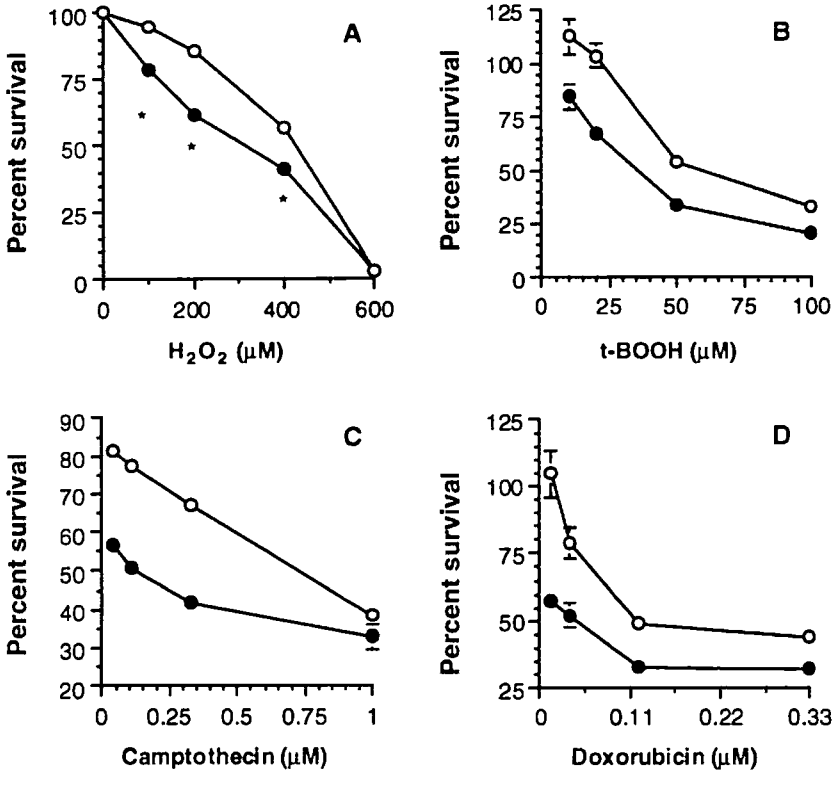

Fig. 21. ***In vitro*** **cytotoxicity of various ROS and ROS-generating anticancer drugs combined with PEG-ZnPP.** SW480 cells were exposed to increasing concentrations of various ROS (A, H_2O_2; B, *t*-BOOH) or ROS-generating anticancer drugs (C, Camptothecin: D, Doxorubicin) for 48 h in the presence (●) or absence (○) of PEG-ZnPP (5 μM). Cell viability was then determined by means of the MTT assay. Values are means ± SE (n = 6-8). *$P < 0.002$.

4.3.3 Induction of Apoptosis by H_2O_2/PEG-ZnPP in SW480 Cells

It has been reported that ROS, including H_2O_2, induce apoptosis (16, 95, 96), and our findings revealed the proapoptotic role of PEG-ZnPP as shown in Chapter 3. Therefore, the combined effect of H_2O_2 and PEG-ZnPP was examined on inducing apoptosis of SW480 cells by use of a fluorescein-labeled Annexin V assay. Figure 22A showed the flow cytometric analyses of apoptotic cells after H_2O_2 (1 mM) or PEG-ZnPP (10 μM) treatment and combination of both. Apoptotic cells were identified as positive staining of FITC labeled Annexin V (FL1-H) and negative staining of PI (FL2-H), which were shown in the lower-right part of the dot plot of each treatment as shown in Figure 22A. Compared with untreated control cells (apoptotic cells of 2.69% in total counted cells), H_2O_2 and PEG-ZnPP each alone induced a apoptosis of 10.23% and 10.21% in total counted cells, respectively (Figure 22B). Interestingly, 44.08% of the total counted cells become apoptotic by the combination treatment of H_2O_2 with PEG-ZnPP (Figure 22B). These results further suggest the synergistic effect of this combination treatment, and that apoptosis is involved in the mechanisms of this combination therapy.

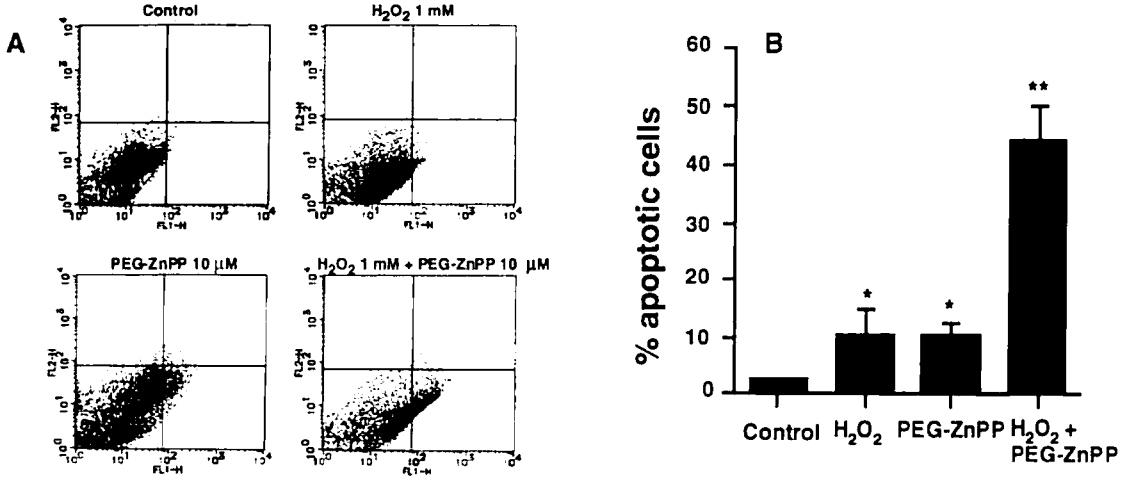

Fig. 22. Induction of apoptosis in SW480 cells by H_2O_2/PEG-ZnPP. Cells were treated with 1 mM of H_2O_2 or 10 μM of PEG-ZnPP and combination of both for 24 h. The number of apoptotic cells was determined by flow cytometry (A), and the percentage of apoptotic cells (per the total number of calculated cells) was shown (B). Values are means ± SE ($n = 4$). $^*P < 0.05$, $^{**}P < 0.005$, versus control.

4.3.4 *In Vivo* Antitumor Activity of PEG-DAO/PEG-ZnPP

To investigate whether this synergy is also effective in *in vivo* system, similar

S180 solid tumor model was used as described in Chapters 2 and 3. The dose, as well as treating period of PEG-DAO system were reduced to half of that shown in Chapter 2, combined with one injection of a low dose of PEG-ZnPP (1.5 mg/kg). PEG-ZnPP was injected i.v. 24 h before administration of PEG-DAO system, to allow the accumulation of PEG-ZnPP and effective inhibition of HO-1 activity in the tumor. Thus, the subsequent addition of ROS from PEG-DAO system will effectively kill the tumor cells that are susceptible to ROS due to the decreased HO-1 activity.

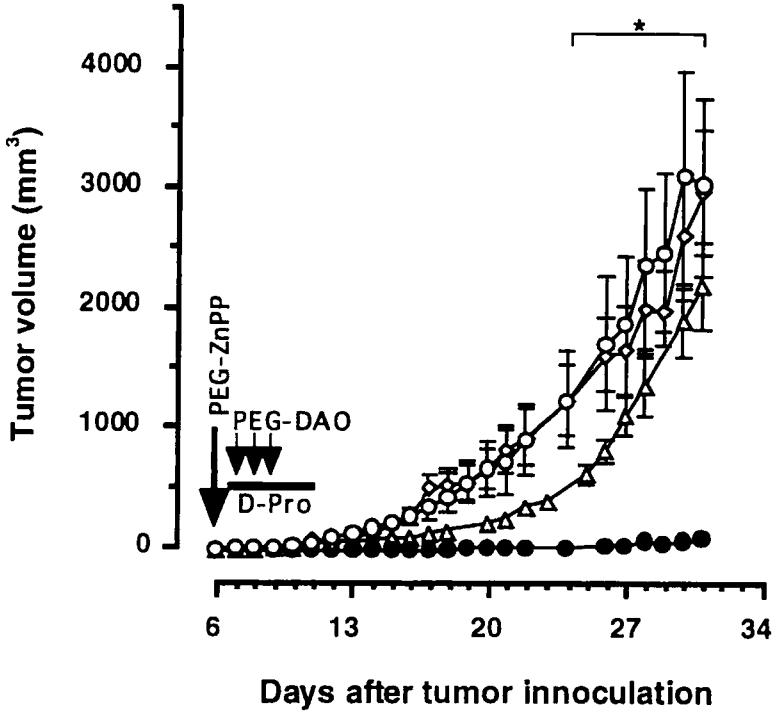

Fig. 23. Antitumor effect of PEG-DAO/PEG-ZnPP in the S180 solid tumor model. S180 cells (2×10^6 cells) were implanted s.c. in ddY mice. *Arrowheads*, administration of PEG-ZnPP (1.5 mg/kg). PEG-DAO system was administered daily from days 7 to 11 after tumor inoculation (PEG-DAO was injected i.v. in the first 3 days at the dose of 0.75 unit/mouse followed by D-proline 0.5 mmol/mouse i.p. injected 4 h after PEG-DAO administration, after which D-proline was injected daily for additional 2 days, at the dose of 0.5 mmol/mouse). ○, control without any treatment; ● PEG-DAO system plus PEG-ZnPP: ◇ PEG-DAO system alone; △ PEG-ZnPP alone. Data are means (n = 8 - 12); bars indicate SE, $*P < 0.01$ (PEG-DAO/PEG-ZnPP group versus control group). #, The complete regression of tumor growth was found in three of eight tumors in PEG-DAO/PEG-ZnPP treatment group. See text for details.

As shown in Figure 23, remarkable (almost complete) suppression of tumor growth was found in mice receiving PEG-DAO system plus PEG-ZnPP. Tumor

growth was suppressed continuously until at least 31 days after tumor inoculation, which was 22 days after the last treatment with PEG-DAO and D-proline. Complete regression of tumor growth was observed in three of eight tumors after treated with PEG-DAO system plus PEG-ZnPP. In contrast, PEG-DAO alone showed no significant antitumor effect, whereas PEG-ZnPP treatment resulted in a slight delay of tumor growth, especially at the early stage of investigation. The average tumor weight on the 31st day after tumor implantation for the groups treated with PEG-DAO/PEG-ZnPP combination, PEG-DAO alone, PEG-ZnPP alone and the untreated control were 0.42 ± 0.17, 3.18 ± 0.73, 2.52 ± 0.36, and 3.34 ± 0.31, respectively. In separate experiments, PEG-PP showed no antitumor activity when either used alone or combined with PEG-DAO (data not shown).

4.3.5 *In Vivo* Induction of Apoptosis by PEG-DAO/PEG-ZnPP

The synergistic effect of PEG-DAO system and PEG-ZnPP on inducing tumor cell apoptosis was further examined *in vivo* by use of the TUNEL assay.

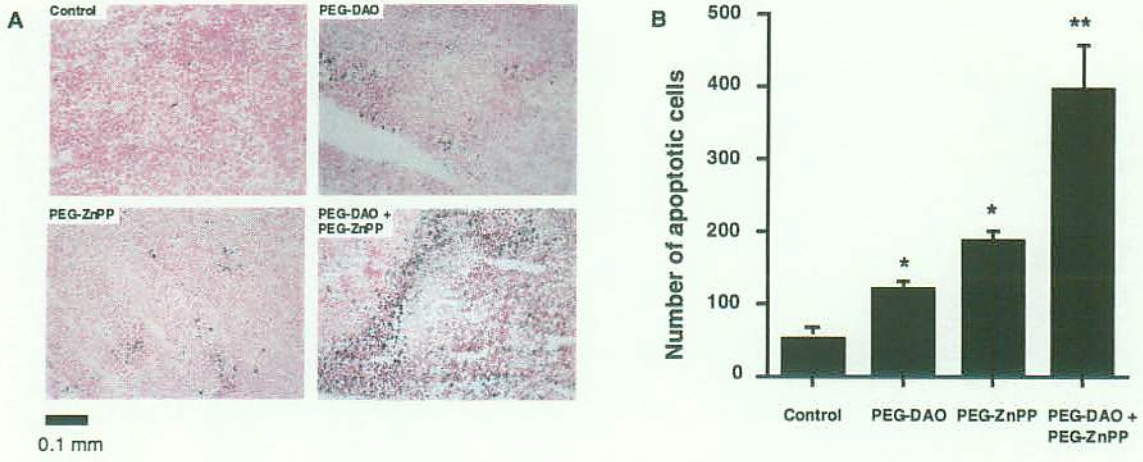

Fig. 24. Induction of apoptosis in S180 solid tumors by PEG-DAO/PEG-ZnPP. Each specimen was collected and examined 24 h after treatment. The treatment protocol was the same as that described in Fig. 23. (A) TUNEL staining for each group. Quantitative analyses of the number of TUNEL-positive cells in each specimen are shown in (B). TUNEL-positive cells were counted in four different fields per sample, and counts were calculated as the number of positive cells per mm^2. Data are means; bars, SE. $*P < 0.02$ versus control; ** $P < 0.05$ versus PEG-DAO alone or PEG-ZnPP alone ($n = 4$ for each group).

As shown in Fig. 24, only a negligible positive staining was identified for the untreated control, whereas a moderate positive staining was detected in either PEG-

DAO or PEG-ZnPP treated specimens. However, strong positive staining were observed in PEG-DAO plus PEG-ZnPP treated S180 tumor tissue (Figure 24A). Morphometric analysis of TUNEL-positive cells in the S180 solid tumors showed that the numbers of positive cells in the control group, the PEG-DAO treated group, the PEG-ZnPP treated group, and the PEG-DAO plus PEG-ZnPP treated group were 53 ± 14/mm^2, 119 ± 14/mm^2, 187 ± 20/mm^2 and 394 ± 71/mm^2, respectively (Figure 24B). These results coincide well with those from the *in vitro* experiments (Figure 22).

4.3.6 Evaluation of Side Effects of PEG-DAO/PEG-ZnPP Treatment

Body Weight Change

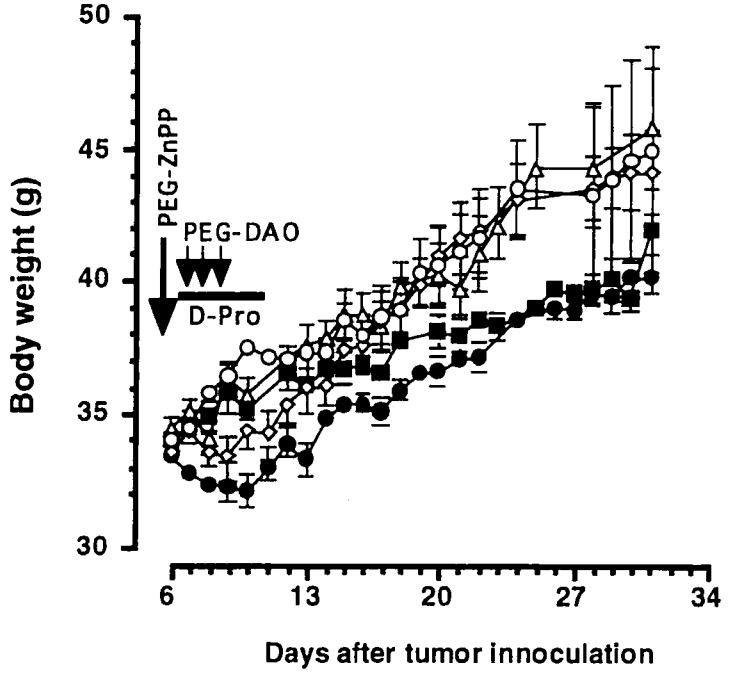

Fig. 25. Body weight changes of ddY mice treated with PEG-DAO, PEG-ZnPP, or combination of both. The treatment protocol was the same as that described for Fig. 23. ○, control mice bearing S180 tumor, no drug treatment: ●, PEG-DAO plus PEG-ZnPP; ◇, PEG-DAO system alone; △, PEG-ZnPP alone; ■, control mice without tumor, no drug treatment. Data are means ± SE (n = 4 - 6).

Figure 25 shows body weight changes in mice receiving different treatments. At the early stage of observation, a slight loss of body weight was found in the group treated by PEG-DAO system plus PEG-ZnPP. However, body weight recovered

gradually at the rate of growth comparable to that of the untreated control mice after the cessation of the treatment. At the later stage of investigation, no significant loss of body weight was observed in mice treated with PEG-DAO system plus PEG-ZnPP, compared with the mice without tumor and given no treatment. Tumor growth appeared to account for the increased body weight of mice treated with PEG-DAO system alone, PEG-ZnPP alone and control group with tumor (see the tumor weight of each group as mentioned in 4.3.4).

Blood Counts and Blood Chemistry

Hematological toxicity of PEG-DAO/PEG-ZnPP treatment was investigated in S180 tumor-bearing mice by use of the routine blood cell count (RBC, WBC, Hb). No significant decreases in any of RBC, WBC counts, or Hb level were found after either treatment, compared with the measures in the untreated control (Table 4). In addition, no significant effects of PEG-DAO/PEG-ZnPP treatment were observed in biochemical assays of major organs (liver, kidney), including plasma ALT, AST, LDH, BUN, and Cr values (Table 4).

. Table 4 Changes in RBC, WBC, hemoglobin and plasma enzyme levels after PEG-DAO/PEG-ZnPP treatment of ddY mice [a]

	RBC (10^4/μl)	WBC (/μl)	Hb (g/l)	BUN (mg/dl)
Control	717.3 ± 56.6	19188 ± 6558	131.1 ± 5.9	21.8 ± 1.5
PEG-DAO (a)	712.5 ± 45.6	25613 ± 8779	137.8 ± 4	20.1 ± 0.5
PEG-ZnPP (b)	778.0 ± 48.2	19700 ± 1794	129.9 ± 7.2	17.3 ± 1.3
a + b	754.3 ± 10.3	16413 ± 1783	140.7 ± 3	17.9 ± 1.4

	Cr (mg/dl)	AST (IU/l/at 37°C)	ALT (IU/l/at 37°C)	LDH (IU/l/at 37°C)
Control	0.15 ± 0.01	233 ± 26.2	34.3 ± 3.2	6046 ± 757
PEG-DAO (a)	0.16 ± 0.01	241 ± 34.9	37.5 ± 8	5165 ± 549
PEG-ZnPP (b)	0.13 ± 0.01	259 ± 21.4	33.3 ± 1.5	8078 ± 1018
a + b	0.16 ± 0.01	269 ± 13.8	35.5 ± 3.1	6816 ± 534

[a] No significant difference was found between each treatment group and the control group in all the selected indices

Values are presented as mean ± SE.

Histological Examination

As shown in Figure 26, tumor tissues showed necrotic changes after either treatment. Most apparent in PEG-DAO system plus PEG-ZnPP treated group. However, no pathological changes were observed in liver, spleen and lung, after PEG-DAO/PEG-ZnPP treatment (data not shown).

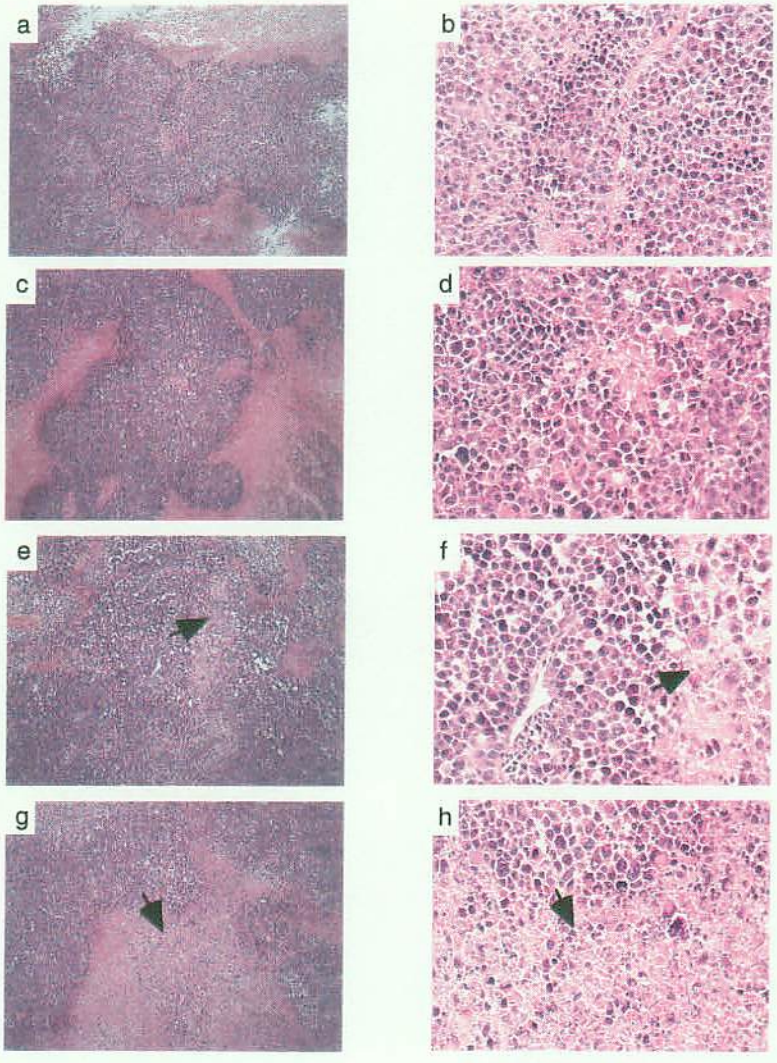

Fig. 26. Histological examination tumors treated by PEG-DAO/PEG-ZnPP. Each specimen was analyzed 24 h after treatment as the protocol described in Fig. 23. (a) and (b), untreated control; (c) and (d), PEG-DAO system alone; (e) and (f), PEG-ZnPP alone; (g) and (h), PEG-DAO system plus PEG-ZnPP. Black arrows indicate the necrotic portions of tumors. (a, c, e, g, × 100 magnification; b, d, f, h, × 400 magnification).

4.4 SUMMARY

In this chapter, I present a new anticancer strategy, named oxidation antitumor therapy, by use of an antioxidant inhibitor (PEG-ZnPP) followed by a ROS-generating system (PEG-DAO system). A preferential synergistic effect of this treatment was achieved, resulting in remarkable tumor regression without any apparent side effect. Based on the EPR effect, PEG-DAO and PEG-ZnPP were selectively delivered to tumor site. Thus, targeted disruption of antioxidative defense of tumor cells by PEG-ZnPP makes them vulnerable to ROS. Consequently, further tumor-targeted delivery of ROS by PEG-DAO system accomplished significant antitumor activity by inducing apoptotic cell death.

CHAPTER 5 DISCUSSIONS

ROS are a group of free radicals, which are molecules with one or more unpaired electrons. Electron acceptors, primarily molecular oxygen, react easily with free radicals, to become oxygen free radicals, named ROS. Because molecular oxygen is ubiquitous in aerobic life, ROS become the primary mediators of cellular free radical reactions. ROS are continuously generated in cells exposed to an aerobic environment, and play important roles in normal and pathological cell metabolism (1, 97). Because of their extremely high reactivity, ROS are potentially harmful, by reacting with, thus damaging protein (98) and DNA (99). Under physiological conditions, damages to oxidisable molecules caused by ROS are reduced by cellular antioxidative defenses (e.g., SOD, catalase, HO-1, glutathione peroxidase) and repair mechanism (100). However, over-burden of ROS, while under pathological conditions such as chronic inflammation (101) and deficiency of antioxidant defense or repair systems, will result in reversible or irreversible tissue injury, consequently leading to various of diseases, including cancer (3, 4, 97).

With Regard to ROS and cancer, the prevailing studies are focus on their roles on carcinogenesis. In the past 10 years, convincing evidence has accumulated that ROS are indeed considered an endogenous class of carcinogens (102-104). In addition, ROS are involved in each stage of cancer development, including initiation, promotion, and progression (97). As mentioned above, overproduction of ROS induces increased damage to DNA, which further triggers mutagenesis via DNA base modifications and DNA helix alterations (97). Moreover, oxidative stress can stimulate the expansion of mutated cell clones by modulating genes related to proliferation and triggering redox-responsive signaling cascades such as epidermal growth factor (EGF), tyrosine phosphorylation and protein kinase C (PKC) (105). In addition, some ROS derivatives, such as peroxynitrite ($ONOO^-$) that is generated from nitric oxide (NO) and O_2^- under pathological conditions and in cancer, also play important roles on tumor angiogenesis and metastasis by activating matrix metalloproteinases (MMPs) (68). These findings, along with clinical trials (106) further consolidate the role of ROS on carcinogenesis and tumor progression.

However, the effect of ROS is dose-dependent, and in a dynamic equilibrium with antioxidant defenses and cellular repair systems (97), their production is a double-edged

sword. While low or intermediate levels of oxidative stress are most effective for triggering mutagenesis and promoting proliferation of cells, high levels of oxidative stress inhibit proliferation by cytotoxic effect (97). More important, the activities of various antioxidative enzymes, such as catalase, glutathione peroxidase, superoxide dismutase (SOD) have been found to be greatly reduced in various tumor cells (107-110), which will increase the vulnerability of tumor cells to ROS. Thus, one can image a new antitumor tactics by selectively delivering excess oxidative stress to tumor cells or targetedly disrupting the antioxidative defense systems of tumor cells. Indeed, several challenges have been done and verified effective by use of this notion (5-9). Along this line, I have challenged this new anticancer strategy by use of a ROS generator (PEG-DAO/D-Proline, see Chapter 2), an antioxidant inhibitor (PEG-ZnPP, see Chapter 3) and both in combination (see Chapter 4). As demonstrated above, remarkable anticancer effect was achieved by each treatment, which suggests the validity of this new anticancer strategy, named oxidation antitumor therapy.

5.1 PEG-DAO/D-PROLINE FOR CANCER THERAPY: A ROS GENERATOR

In this study (Chapter 2), remarkable antitumor activity was demonstrated of pegylated DAO plus D-proline on mouse solid tumor model (Figure 7). In regard to the side effects, even though some side effects may be induced by PEG-DAO/D-proline treatment as evaluated by body weight change, it appears to be slight and transient (Figure 8). This effect is similar to that observed in the case of PEG-conjugated XO (6). Key findings of the present study are as following: (i) tumor-targeted delivery of an H_2O_2-generating enzyme (DAO) can be accomplished, and (ii) generation of H_2O_2 by exogenous administration of its substrate (D-proline) resulted in tumor regression.

To deliver DAO to tumor tissue, the concept of the EPR effect was utilized, which is applicable to macromolecules and lipids in a variety of solid tumors (41, 42, 44, 48-54). In the phenomenon termed the EPR effect, biocompatible macromolecules and lipids preferentially and spontaneously leak out of tumor vessels, and remain accumulated without being removed, in tumor tissues. This EPR effect is a molecular size-dependent phenomenon, and it operates at the molecular size above 40 kDa (41-46). This molecular dependency on tumor accumulation exhibits a reverse correlation to the renal clearance of the compounds (41, 52-54). Therefore, the EPR effect is observed for any biocompatible macromolecule with a molecular size larger than the renal

excretion threshold.

As expected, native DAO (39 kDa) was rapidly cleared from the circulation after i.v. injection (Figure 5 and inset) and did not accumulate well in tumor tissue (Figure 6). To obviate this drawback, PEG-DAO was prepared, which showed an increased *in vivo* half-life (Figure 5 inset and Table 2). More important, PEG-DAO accumulated more selectively in tumor tissue (Figure 6). The relative concentration of DAO was about 7.4-fold and 9.1-fold higher in the tumor and plasma, respectively, after PEG-DAO injection compared with untreated control. These findings clearly indicate that PEG-DAO is delivered to tumor tissue according to the EPR effect. Previously, similar beneficial effects was found of polymer conjugate of various polymers (41, 44, 53) including pyran copolymer, succinylated keratin, styrene maleic acid copolymer, and poly(vinyl alcohol).

PEG-DAO alone or D-proline alone did not show any antitumor activity: the cytotoxic effect was observed only when DAO and D-proline were both present. The new type of cancer therapy described here depends on selective targeting of the H_2O_2-generating enzyme (DAO) to the tumor site, the enzyme converting a subsequently supplied pharmacologically inert prodrug (D-proline) to a highly cytotoxic metabolite, H_2O_2. From *in vitro* experiments, the LC_{50} values for D-proline and D-alanine in the presence of 10 mU/ml PEG-DAO were determined to be 0.3 mM and 3.6 mM, respectively (Figure 4). More important, these values are much higher than those in plasma, i.e., the plasma concentrations of D-proline and D-alanine in humans have been reported as 0.22 and 0.61 μM, respectively (111). Via tumor-targeted delivery of PEG-DAO, the generation of H_2O_2 could be regulated by exogenous administration of D-amino acids. This notion is further supported by a tumor-specific increase in TBARS, which is a marker of oxidative metabolites (Figure 9).

Catalase plays a central function in the antioxidant defense of many organisms, as do other enzymes such as superoxide dismutase and glutathione peroxidase, as H_2O_2 is degraded to H_2O (112). Catalase activity has been found to be significantly reduced in various tumor cells (107). Sato et al. demonstrated that such reduced catalase activity is due to a marked depression of catalase gene expression at the level of transcription (110). In addition, down-regulation of catalase gene expression has been observed in the doxorubicin-resistant acute myelogenous leukemia subline (AML-2/DX100), which overexpresses multidrug resistance-associated protein (113). The multidrug resistance

cell line AML-2/DX100, shows resistance to doxorubicin, daunorubicin, and vincristine but is paradoxically sensitive to H_2O_2. These findings may lend further support to the validity of the present approach utilizing H_2O_2-generating enzymes for antitumor treatment.

5.2 PEG-ZnPP FOR CANCER THERAPY: AN ANTIOXIDANT INHIBITOR

The study described in Chapter 3 revealed the antitumor activity of a water-soluble HO inhibitor, PEG-ZnPP. *In vitro* experiments showed that PEG-ZnPP had cytotoxic effects on cultured SW480 cells, which express HO-1, whereas PEG-PP, a zinc-free analogue of PEG-ZnPP having no HO inhibitory activity, did not (Figure 11). Coincubation of cells with the antioxidant NAC reduced the cytotoxicity of PEG-ZnPP. In addition, flow cytometric analysis using an oxidant-sensitive fluorescence probe (DCDHF) revealed increased intracellular oxidant levels after PEG-ZnPP treatment (Figure 12). Thus, PEG-ZnPP exerts its cytotoxic effect on tumor cells by inhibiting HO activity, which leads to increased production of toxic oxidants. Reactive oxidants thus formed could trigger the apoptotic pathway (Figure 13) by activating the caspase-3 cascade, as recently demonstrated for native ZnPP (114). The antiapoptotic role of HO-1 was further demonstrated in this study by using siRNA (Figure 13B), which specifically inhibits HO-1 activity by targeted annealing with HO-1 mRNA (90). Among the products of the HO reaction, bilirubin could function as an antioxidant and/or free radical scavenger (35-37). In this context, it was recently found that native ZnPP treatment reduced the intracellular bilirubin level, and that exogenous bilirubin supplementation could compensate for the cytotoxic effect of ZnPP (114).

As a more important finding, PEG-ZnPP showed marked antitumor activity *in vivo* even after systemic administration to tumor-bearing mice (Figure 15). In contrast, PEG-PP did not show any antitumor activity at the same dose range. These results correlate well with the findings that PEG-ZnPP, but not PEG-PP, significantly suppressed intratumor HO activity (Figure 18) and induced apoptosis of tumor cells (Figure 17). Inhibition of HO activity makes tumor cells susceptible to ROS derived from the metabolism of the cells themselves and ROS from the inflammatory cells of the host (40, 60), by reducing the antioxidant bilirubin level. Consequently tumor cells undergo apoptosis (as seen in Figure 17) via the caspase-3-dependent pathway, as mentioned above. An anti-inflammatory effect of HO-1 (39) may also be involved in

PEG-ZnPP-mediated antitumor activity. CO derived from heme degradation was recently reported to potentially inhibit the production of the proinflammatory cytokine tumor necrosis factor-α (TNF-α) from activated macrophages (115). Therefore, inhibition of HO-1 by PEG-ZnPP may enhance the inflammatory response in tumor tissues by increasing TNF-α production and hence reinforce the host defense system. In addition, Yang et al reported that ZnPP induced apoptosis of hamster fibroblasts (HA-1) by up-regulating p53 expression, via ZnPP-mediated Egr-1 binding (116), which suggests an alternative pathway of ZnPP-induced apoptosis. However, whether this mechanism is involved in the increased apoptosis seen after PEG-ZnPP treatment observed in the present work needs further investigation.

The antitumor activity of PEG-ZnPP may establish a new role for this compound in cancer treatment. In this regard, targeted delivery of PEG-ZnPP to tumor tissues is critical, because nonspecific distribution of PEG-ZnPP may cause systemic oxidative stress by reducing the antioxidant capacity of normal organs. Although radioactivity derived from ^{65}Zn in radiolabeled PEG-ZnPP was detected at the highest level in spleen compared with other organs and tissues (Figure 14 C), the HO activity (Figure 18) and the apoptotic index (Figure 17) in spleen were unchanged by PEG-ZnPP treatment. These findings suggest that the bioavailability of PEG-ZnPP in the spleen may be limited, probably because of the special histological characteristics of this organ; PEG-ZnPP that accumulates in the spleen may be captured, degraded, or inactivated by the rich RES, including elements such as macrophages, as reported for other macromolecular compounds. This may be the case as well for liver, an organ also rich in RES (93). ZnPP is also known to have toxic effects on the bone marrow by inhibiting the growth of erythroid and myeloid cells (94). However, we did not find any significant changes in blood cells after PEG-ZnPP treatment (Table 3). These results, together with those for body weight change (Figure 16), indicate that systemic side effects of PEG-ZnPP treatment seem to be negligible.

With exception for spleen and liver, PEG-ZnPP preferentially accumulated in solid tumor tissue (Figure 14C). Pharmacokinetic study showed that the amount of PEG-ZnPP in tumor tissue increased in a time-dependent manner (Figure 14B), whereas the amount of PEG-ZnPP in circulation gradually decreased (Figure 14A). This finding suggests that PEG-ZnPP accumulates or is deposited in solid tumor tissues after systemic administration. A similar accumulation of biocompatible macromolecules

has been reported for a variety of solid tumor tissues, which may be explained by the unique characteristics of tumor vasculature, named EPR effect (41, 54, 117, 118). As described above, this EPR effect can be observed for macromolecules having an apparent molecular size larger than 40 KDa, i.e., large enough to escape from renal clearance (41-46). As expected, the AUC for PEG-ZnPP (apparent M_r > 70 KDa in aqueous media as a micelle formation; see ref. 84) showed a 40-fold increase compared with that for native ZnPP (M_r = 626) (Figure 14A). Thus, PEG-ZnPP is delivered to tumor tissue according to the EPR effect, and hence it effectively, and selectively inhibits HO activity in tumor. Consequently, remarkable suppression of tumor growth was achieved, at least in part by the increased endogenous ROS due to the reduced activity of HO-1 via an apoptosis pathway. The effect of PEG-ZnPP described here is consistent with the antitumor strategy of oxidation therapy.

5.3 COMBINATION OF ROS GENERATOR AND ANTIOXIDANT INHIBITOR FOR CANCER THERAPY

In Chapter 4, the antitumor effect of a combination treatment was described, by use of the PEG-DAO/D-proline ROS generating system and the antioxidant inhibitor PEG-ZnPP. Separate treatment by PEG-DAO/D-proline or PEG-ZnPP showed very little effect on tumor growth suppression in a murine solid tumor model (Figure 23). However, superior antitumor effect of the combination therapy of PEG-DAO/D-proline plus PEG-ZnPP was found under the same treatment conditions, compared to any separate treatment and control (Figure 23). These results revealed the synergistic antitumor effect of these two compounds. The findings from *in vitro* experiments further evidenced the synergistic effect of this combination treatment (Figure 20, 21, 22). PEG-ZnPP at 5 or 10 μM, which is lower than its cytotoxic dose (Figure 11), dramatically enhanced the intracellular ROS generation (Figure 20), cytotoxicity (Figure 21A) and apoptosis induction (Figure 22) of H_2O_2. Furthermore, the synergistic effect was also observed on *t*-BOOH, camptothecin, and doxorubicin related cytotoxicity by combined with PEG-ZnPP (Figure 21B, C, D). It is well known that most of the conventional anticancer drugs such as camptothecin and doxorubicin exhibit antitumor activity by generating ROS (18). Thus, these results suggest that the synergy does not happen only in this experiment, but is common for any ROS-generating anticancer drugs with PEG-ZnPP.

One of the major problems faced to the traditional antitumor chemotherapy is how to reduce the adverse side effects. To find the optimal dose of any anticancer drug that is effective to treat cancer but will not induce severe side effects, is a very difficult task for clinical oncologists. Combination of different antitumor drugs may attenuate the unexpected side effects by lowering the dose of separate drugs; and moreover, enhance the antitumor efficacy by utilizing the addictive and/or synergistic effect of different drugs. In fact, combination therapy is commonly used in clinics. In this study, this notion was further challenged on oxidation therapy, by use of the above-mentioned PEG-DAO system and PEG-ZnPP. The dose and period of administration of PEG-DAO system used in this experiment were reduced to half as that used in the experiment of PEG-DAO system alone (see Chapter 2), which did not show apparent antitumor effect. However, marked tumor growth suppression was found by combined with one injection of PEG-ZnPP with a low dose (1.5 mg/kg) (Figure 23). More important, no or very little, if any at all, adverse side effect was observed in this treatment, as evidenced by the chosen parameters such as body weight loss, blood counts and blood chemistry, and histological examination (Figure 25, Table 4). This is consistent with the concept of combination chemotherapy. In addition, the reagents used in this experiment are pegylated macromolecular compounds, thus the EPR effect will further facilitate their effects while reducing side effects, by tumor selective targeting, as discussed above (41-54).

Another major obstacle for the successful antitumor therapy is the development of multidrug resistance (MDR), which is mainly associated with the active efflux of anticancer drugs mediated by the P-glycoprotein (Pgp) of MDR cells (119). Pgp expression has been found down regulated in tumor spheroids by ROS through tyrosine kinase signaling pathway (120). It has also been reported that macromolecular drugs are independent from the Pgp-dependent efflux process, because the rapid efflux of drugs by Pgp depends on appropriate intracellular localization of the drugs, to access to the Pgp, which does not fit to macromolecules that are taken up by the endocytosis-dependent pathway (121, 122). In addition, as discussed earlier, a MDR cell line with decreased expression and activity of catalase, shows resistance to doxorubicin, daunorubicin, and vincristine but is sensitive to ROS (e.g., H_2O_2 and *t*-butyl hydroperoxide) (113); and more important, various tumor cells have lower catalase activity (107, 110). Therefore, it may be reasonable and valid that above-described

combination antitumor therapy, by use of the polymer-conjugated ROS generators (e.g., PEG-DAO system) and inhibitors of antioxidative enzymes (e.g., PEG-ZnPP). Furthermore, this combination therapy might be extended to conventional ROS-related anticancer drugs such as camptothecin, doxorubicin and vinblastine, by combined with PEG-ZnPP as a ROS enhancer.

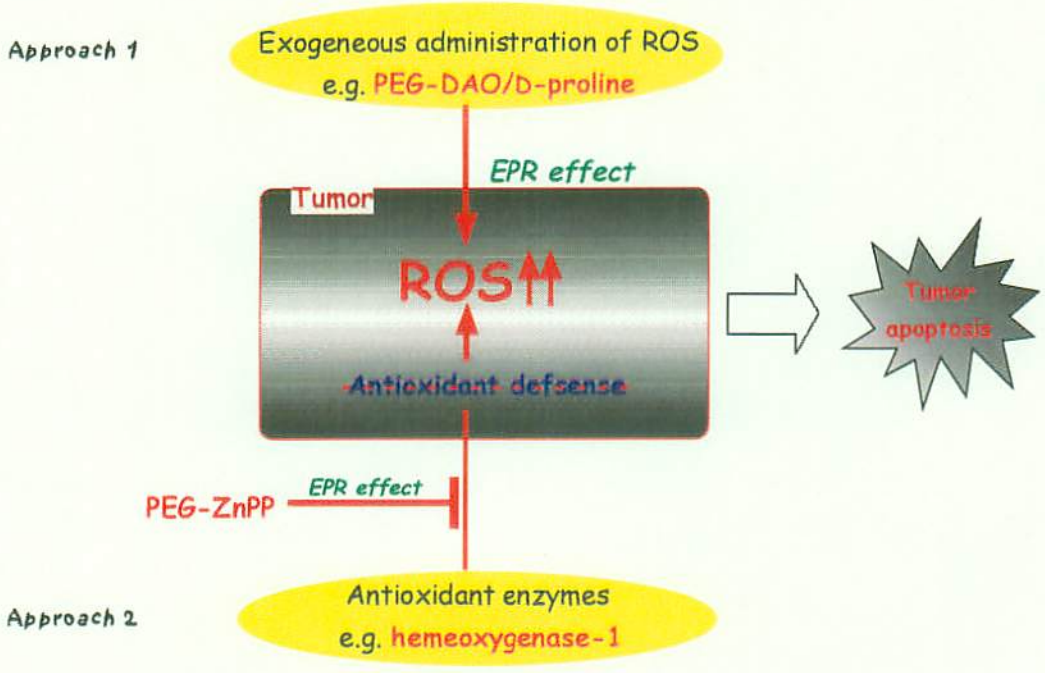

Fig. 27. Scheme of the new anticancer strategy: oxidation therapy. The ROS accumulation in tumor cells is induced by two approaches; one is through exogenous delivery, which can be achieved by ROS-generating enzymes (e.g., PEG-DAO system); another way is by inhibiting the antioxidative defense system of tumor cells (e.g., HO-1 inhibition via PEG-ZnPP). EPR effect is necessary for the targeted delivery to tumor in both approaches. Thus increased ROS in tumor kill the tumor cells via an apoptosis related pathway. Consequently, remarkable and favorable antitumor effect is achieved without apparent side effect (see text for details).

5.4 SUMMARY

ROS, a group of highly reactive molecules, exhibits highly important, yet paradoxical role on tumor. On the one hand, it can damage DNA, thus initiate and promote cancer development. On the other hand, it can serve as a tumor terminator if it is at very high concentration, due to its cytotoxic effect. Moreover, although being not described here, the highly elevated level of NO production in tumor will further

facilitate the antitumor effects of ROS by generating more reactive species such as $ONOO^-$, which will be a combined effector in this anticancer tactics. How to perform the tumor-selective generation of ROS is the key point for this goal. While ROS production can be targeted to tumor tissues and remain accumulated there by polymer conjugation, as shown in this work as well as our previous work (6), successful antitumor effect can be achieved without apparent side effects by taking advantage of the EPR effect of macromolecules in solid tumor (see figure 27). Another important rationale of this study is that tumor cells frequently possess very little antioxidative enzymes (e.g., catalase; see refs. 107, 110), which makes them very vulnerable to oxidative stresses. Thus, the new antitumor strategy, oxidation therapy, might be a promising approach for clinical anticancer trials in the future, while warrants further investigation.

REFERENCES

1 Davies, K. J. Oxidative stress: the paradox of aerobic life. Biochem. Soc. Symp., *61:* 1-31, 1995.

2 Sundaresan, M., Yu, Z. X., Ferrans, V. J., Irani, K., and Finkel T. Requirement for generation of H_2O_2 for platelet-derived growth factor signal transduction. Science, *270:* 296-299, 1995.

3 McCord, J. M. The evolution of free radicals and oxidative stress. Am. J. Med., *108:* 652-659, 2000.

4 Maeda, H., and Akaike, T. Oxygen free radicals as pathogenic molecules in viral diseases. Proc. Soc. Exp. Biol. Med., *198:* 721-727, 1991.

5 Ben-Yoseph, O., and Ross, B. D. Oxidation therapy: the use of a reactive oxygen species-generating enzyme system for tumour treatment. Br. J. Cancer, *70:* 1131-1135, 1994.

6 Sawa, T., Wu, J., Akaike, T., and Maeda, H. Tumor-targeting chemotherapy by a xanthine oxidase-polymer conjugate that generates oxygen-free radicals in tumor tissue. Cancer Res., *60:* 666-671, 2000.

7 Yoshikawa, T., Kokura, S., Tanaka, K., Naito, Y., and Kondo, M. A novel cancer therapy based on oxygen radicals. Cancer Res., *55:* 1617-1620, 1995.

8 Stegman, L. D., Zheng, H., Neal, E. R., Ben-Yoseph, O., Pollegioni, L., Pilone, M. S., and Ross, B. D. Induction of cytotoxic oxidative stress by D-alanine in brain tumor cells expressing *Rhodotorula gracilis* D-amino acid oxidase: a cancer gene therapy strategy. Hum. Gene Ther., *9:* 185-193, 1998.

9 Huang, P., Feng, L., Oldham, E. A., Keating, M. J., and Plunkett, W. Superoxide dismutase as a target for the selective killing of cancer cells. Nature, *407:* 390-395,

2000.

10 Beckman, K. B., and Ames. B. N. Oxidative decay of DNA. J. Biol. Chem., *272:* 19633-19636, 1997.

11 Berlett, B. S., and Stadtman. E. R. Protein oxidation in aging, disease, and oxidative stress. J. Biol. Chem., *272:* 20313-20316, 1997.

12 Halliwell, B., and Gutteridge, J. M. Free radicals, lipid peroxidation, and cell damage. Lancet. *2:* 1095, 1984.

13 Bladier, C., Wolvetang, E. J., Hutchinson, P., de Haan, J. B., and Kola, I. Response of a primary human fibroblast cell line to H_2O_2: senescence-like growth arrest or apoptosis? Cell Growth Differ., *8:* 589-598, 1997.

14 Matsura, T., Kai, M., Fujii, Y., and Yamada, K. Hydrogen peroxide-induced apoptosis in HL-60 cells requires caspase-3 activation. Free Radic. Res., *30:* 73-83, 1999.

15 Yamakawa, H., Ito, Y., Naganawa, T., Banno, Y., Nakashima, S., Yoshimura, S., Sawada, M., Nishimura, Y., Nozawa, Y., and Sakai, N. Activation of caspase 9 and 3 during H_2O_2-induced apoptosis of PC12 cells independent of ceramide formation. Neurol. Res., *22:* 556-564, 2000.

16 Suhara, T., Fukuo, K., Sugimoto, T., Morimoto, S., Nakahashi, T., Hata, S., Shimizu, M., and Ogihara, T. Hydrogen peroxide induces up-regulation of Fas in human endothelial cells. J. Immunol. *160:* 4042-4047, 1998.

17 Ren, J. G., Xia, L. H., Just, T., and Dai, Y. R. Hydroxyl radical-induced apoptosis in human tumor cells is associated with telomere shortening but not telomerase inhibition and caspase activation. FEBS Lett. *488:* 123-132, 2001.

18 Simizu, S., Takada, M., Umezawa, K., and Imoto, M. Requirement of caspase-3 (-

like) protease-mediated hydrogen peroxide production for apoptosis induced by various anticancer drugs. J. Biol. Chem., *273:* 26900-26907, 1998.

19 Green, H. N., and Westrop, J. W. Hydrogen peroxide and tumour therapy. Nature. *181:* 128-129, 1958.

20 Sugiura, K. Effect of hydrogen peroxide on transplanted rat and mouse tumours. Nature. *182:* 1310-1311, 1958.

21 Mealey, J. Jr. Regional infusion of vinblastine and hydrogen peroxide in tumor-bearing rats. Cancer Res.. *25:* 1839-1843, 1965.

22 Kaibara, N., Ikeda, T., Hattori. T.. and Inokuchi, K. Experimental studies on enhancing the therapeutic effect of mitomycin-C with hydrogen peroxide. Jpn. J. Exp. Med., *41:* 323-329, 1971.

23 Makino, S., and Tanaka, T. The cytological effects of chemicals on ascites sarcomas. II. Selective damage to tumor cells by $CaCl_3$ and H_2O_2. Gann. *44:* 39-46, 1953.

24 Nathan, C. F., and Cohn, Z. A. Antitumor effects of hydrogen peroxide in vivo. J. Exp. Med.. *154:* 1539-1553, 1981.

25 Konno, R.. and Yasumura, Y. D-Amino acid oxidase and its physiological functions. Int. J. Biochem., *24:* 519-524, 1992.

26 Schacter, B. A. Heme catabolism by heme oxygenase: Physiology, regulation, and mechanism of action. Semin. Hematol.. *25:* 349-369, 1988.

27 Maines, M. D. Heme oxygenase: function, multiplicity, regulatory mechanisms, and clinical applications. FASEB J., *2:* 2557-2568, 1988.

28 Tenhunen, R., Marver, H. S.. and Schmid, R. The enzymatic catabolism of

hemoglobin: stimulation of microsomal heme oxygenase by hemin. J. Lab Clin. Med., *75:* 410-421, 1970.

29 Shibahara, S. Regulation of heme oxygenase gene expression. Semin. Hematol., *25:* 370-376, 1988.

30 Keyse, S. M., and Tyrrell, R. M. Heme oxygenase is the major 32-kDa stress protein induced in human skin fibroblasts by UVA radiation, hydrogen peroxide, and sodium arsenite. Proc. Natl. Acad. Sci. U. S. A., *86:* 99-103, 1989.

31 Mitani, K, Fujita, H., Fukuda, Y., Kappas, A., and Sassa, S. The role of inorganic metals and metalloporphyrins in the induction of haem oxygenase and heat-shock protein 70 in human hepatoma cells. Biochem. J., *290:* 819-825, 1993.

32 Motterlini, R., Foresti, R., Bassi, R., Calabrese, V., Clark, J. E., and Green, C. J. Endothelial heme oxygenase-1 induction by hypoxia. Modulation by inducible nitric oxide synthase and S-nitrosothiols. J. Biol. Chem., *275:* 13613-13620, 2000.

33 Foresti, R., Clark, J. E., Green, C. J., and Motterlini, R. Thiol compounds interact with nitric oxide in regulating heme oxygenase-1 induction in endothelial cells. Involvement of superoxide and peroxynitrite anions. J. Biol. Chem., *272:* 18411-18417, 1997.

34 Doi, K., Akaike, T., Fujii, S., Tanaka, S., Ikebe, N., Beppu, T., Shibahara, S., Ogawa, M., and Maeda, H. Induction of haem oxygenase-1 by nitric oxide and ischaemia in experimental solid tumours and implications for tumour growth. Br. J. Cancer, *80:* 1945-1954, 1999.

35 Farrera, J. A., Jauma, A., Ribo, J. M., Peire, M. A., Parellada, P. P., Roques-Choua, S., Bienvenue, E., and Seta, P. The antioxidant role of bile pigments evaluated by chemical tests. Bioorg. Med. Chem., *2:* 181-185, 1994.

36 Minetti, M., Mallozzi, C., Di Stasi, A. M., and Pietraforte, D. Bilirubin is an

effective antioxidant of peroxynitrite-mediated protein oxidation in human blood plasma. Arch. Biochem. Biophys.. *352:* 165-174. 1998.

37 Dore, S., Takahashi, M., Ferris, C. D.. Zakhary. R., Hester. L. D., Guastella, D., and Snyder. S. H. Bilirubin, formed by activation of heme oxygenase-2, protects neurons against oxidative stress injury. Proc. Natl. Acad. Sci. U.S.A., *96:* 2445-2450. 1999.

38 Petrache, I., Otterbein, L. E., Alam. J., Wiegand, G. W., and Choi, A. M. Heme oxygenase-1 inhibits TNF-alpha-induced apoptosis in cultured fibroblasts. Am. J. Physiol., *278:* L312-L319, 2000.

39 Otterbein. L. E., Mantell, L. L., and Choi, A. M. Carbon monoxide provides protection against hyperoxic lung injury. Am. J. Physiol.. *276:* L688-L694, 1999.

40 Doi, K., Akaike, T., Horie. H., Noguchi. Y. Fujii, S., Beppu, T., Ogawa, M., and Maeda. H. Excessive production of nitric oxide in rat solid tumor and its implication in rapid tumor growth. Cancer, 77: 1598-1604, 1996.

41 Matsumura. Y., and Maeda, H. A new concept for macromolecular therapeutics in cancer chemotherapy: mechanism of tumoritropic accumulation of proteins and the antitumor agent SMANCS. Cancer Res., *46:* 6387-6392, 1986.

42 Maeda, H., Seymour, L. W., and Miyamoto. Y. Conjugates of anticancer agents and polymers: advantages of macromolecular therapeutics in vivo. Bioconjug. Chem., *3:* 351-362, 1992.

43 Kojima. Y., Haruta. A., Imai, T., Otagiri, M., and Maeda, H. Conjugation of Cu,Zn-superoxide dismutase with succinylated gelatin: pharmacological activity and cell-lubricating function. Bioconjug. Chem., *4:* 490-498, 1993.

44 Noguchi. Y., Wu, J., Duncan, R., Strohalm, J., Ulbrich, K., Akaike. T., and Maeda, H. Early phase tumor accumulation of macromolecules: a great difference in

clearance rate between tumor and normal tissues. Jpn. J. Cancer Res., *89:* 307-314, 1998.

45 Seymour, L. W., Miyamoto, Y., Maeda, H., Brereton, M., Strohalm, J., Ulbrich, K., and Duncan, R. Influence of molecular weight on passive tumour accumulation of a soluble macromolecular drug carrier. Eur. J. Cancer, *31A:* 766-770, 1995.

46 Tsutsumi, Y., Kihara, T., Yamamoto, S., Kubo, K., Nakagawa, S., Miyake, M., Horisawa, Y., Kanamori, T., Ikegami, H., and Mayumi, T. Chemical modification of natural human tumor necrosis factor-α with polyethylene glycol increases its anti-tumor potency. Jpn. J. Cancer Res. *85:* 9-12, 1994.

47 Pyatak, P. S., Abuchowski, A., and Davis, F. F. Preparation of a polyethylene glycol: superoxide dismutase adduct, and an examination of its blood circulating life and anti-inflammatory activity. Res. Commun. Chem. Pathol. Pharmacol. *29:* 113-127, 1980.

48 Duncan, R. Polymer conjugates for tumour targeting and intracytoplasmic delivery. The EPR effect as a common gateway? Pharm. Sci. Technol. Today, *2:* 441-449, 1999.

49 Muggia, F. M. Doxorubicin-polymer conjugates: further demonstration of the concept of enhanced permeability and retention. Clin. Cancer Res., *5:* 7-8, 1999.

50 Marecos, E., Weissleder, R., and Bogdanov, A. Jr. Antibody-mediated versus non-targeted delivery in human small cell lung carcinoma model. Bioconjug. Chem., *9:* 184-191, 1998.

51 Maeda, H., Takeshita, J., and Kanamaru, R. A lipophilic derivative of neocarzinostatin. A polymer conjugation of an antitumor protein antibiotic. Int. J. Peptide Protein Res., *14:* 81-87, 1979.

52 Maeda, H., and Matsumura, Y. Tumoritropic and lymphotropic principles of

macromolecular drugs. Crit. Rev. Ther. Drug Carrier Syst., *6:* 193-210, 1989.

53 Maeda, H., and Kojima, Y. Polymer-drug conjugates. *In:* R. Arshady (ed.). Desk Reference of Functional Polymers: Synthesis and Application, pp. 753-767. Washington, DC: American Chemical Society, 1997.

54 Maeda, H. SMANCS and polymer-conjugated macromolecular drugs: advantages in cancer chemotherapy. Adv. Drug Deliv. Rev., *46:* 169-185, 2001.

55 Folkman, J. Tumor angiogenesis: therapeutic implications. N. Engl. J. Med., *285:* 1182-1186, 1971.

56 Folkman, J. and Shing, Y. Angiogenesis. J. Biol. Chem., *267:* 10931-10934, 1992.

57 Maeda, H., Matsumura, Y. and Kato, H. Purification and identification of [hydroxyprolyl^3] bradykinin in ascitic fluid from a patient with gastric cancer. J. Biol. Chem., *263:* 16051-16054, 1988.

58 Matsumura, Y., Kimura, M., Yamamoto, T., and Maeda, H. Involvement of the kinin-generating cascade in enhanced vascular permeability in tumor tissue. Jpn. J. Cancer Res., *79:* 1327-1334, 1988.

59 Matsumura, Y., Maruo., K., Kumura, M., Yamamoto, T., Konno, T., and Maeda, H. Kinin-generating cascade in advanced cancer patients and in vitro study. Jpn. J. Cancer Res., *82:* 732-741, 1991.

60 Wu, J., Akaike, T., and Maeda, H. Modulation of enhanced vascular permeability in tumors by bradykinin antagonist, a cyclooxygenase inhibitor, and a nitric oxide scavenger. Cancer Res., *58:* 159-165m 1998.

61 Maeda, H., Noguchi, Y., Sato, K., and Akaike, T. Enhanced vascular permeability in solid tumor is mediated by nitric oxide and inhibited by both nitric oxide scavenger and nitric oxide synthase inhibitor. Jpn. J. Cancer Res., *85:* 331-334.

1994.

62 Senger, D. R., Galli, S. J., Dovorak, A. M., Perruzzi, C. A., Harvey, V. S. and Dvorak, H. F. Tumor cells secrete a vascular permeability factor that promotes accumulation of ascites fluid. Science, *219:* 983-985, 1983.

63 Ferrara, N. and Henzel, W. J. Pituitary follicular cells secrete a novel heparin-binding growth factor specific for vascular endothelial cells. Biochem. Biophys. Res. Commun. *161:* 851-858, 1989.

64 Rosenthal, R. A., Megyesi, J. F., Henzel, W. J., Ferrara, N. and Folkman, J. Conditioned medium from mouse sarcoma 180 cells contains vascular endothelial growth factor. Growth Factors *4:* 53-59, 1990.

65 Leung, D. W., Cachianes, G., Kuang, W-J., Goeddel, D. V. and Ferrara, N. Vascular endothelial growth factor is a secreted angiogenic mitogen. Science *246:* 1306-1309, 1989.

66 Keck, P. J., Hauser, S. D., Krivi, G., Sanzo, K., Warren, T., Feder, J. and Connolly, D. T. Vascular permeability factor, an endothelial cell mitogen related to PDGF. Science *246:* 1309-1312, 1989.

67 Reichman, H. R., Farrell, C. L. and Del Maestro, F. R. Effect of steroids and nonsteroid anti-inflammatory agents on vascular permeability in a rat glioma model. J. Neurosurg. *65:* 233-237, 1986.

68 Wu, J., Akaike, T., Hayashida, K., Okamoto, T., Okuyama, A. and Maeda, H. Enhanced vascular permeability in solid tumor involving peroxynitrite and matrix metalloproteinases. Jpn. J. Cancer Res. *92:* 439-451, 2001.

69 Suzuki, M., Takahashi, T. and Sato, T. Medial regression and its functional significance in tumor–supplying host arteries. Cancer, *59:* 444-450, 1987.

70 Skinner, S. A., Tutton, P. J. M., and O'brien, E. Microvascular architecture of experimental colon tumors in the rats. Cancer Res., *50:* 2411-2417, 1991.

71 Zalipsky, S. Functionalized poly(ethylene glycol) for preparetion of biologically relevant conjugates. Bioconjugate Chem. *6:* 150-165, 1995.

72 Harris, J. M. (ed.). Poly(ethylene glycol) chemistry: biotechnical and biomedical applications. Plenum Press, New York, 1992.

73 Yagi, K. Reaction mechanism of D-amino acid oxidase. Adv. Enzymol. Relat. Areas Mol. Biol., *34:* 41-78, 1971.

74 Kimura, M., Matsumura, Y., Miyauchi, Y., and Maeda, H. A new tactic for the treatment of jaundice: An injectable polymer-conjugated bilirubin oxidase. Proc. Soc. Exp. Biol. Med., *188:* 364-369, 1988.

75 Fields, R. The rapid determination of amino groups with TNBS. Methods Enzymol. *25:* 464-468, 1972.

76 Bernt, E., and Bergmeyer, E. R. Inorganic peroxides. *In*: H. Bergmeyer (ed.), Methods of Enzymatic Analysis, Vol. 4, pp. 2246-2247. New York: Academic Press, 1974.

77 Mosmann, T. Rapid colorimetric assay for cellular growth and survival: application to proliferation and cytotoxicity assay. J. Immunol. Methods, *65:* 55-63, 1983.

78 D'Aniello, A., D'Onofrio, G., Pischetola, M., D'Aniello, G., Vetere, A., Petrucelli, L., and Fisher, G. H. Biological role of D-amino acid oxidase and D-aspartate oxidase. Effects of D-amino acids. J. Biol. Chem., *268:* 26941-26949, 1993.

79 Yamaoka, K., Tanigawara, Y., Nakagawa, T., and Uno, T. A pharmacokinetic analysis program (MULTI) for microcomputer. J. Pharmacobiodyn. *4:* 879-885, 1981.

80 Ohkawa, H., Ohishi, N., and Yagi, K. Assay for lipid peroxides in animal tissues by thiobarbituric acid reaction. Anal. Biochem., *95:* 351-358, 1979.

81 Buege, J. A., and Aust, S. D. Microsomal lipid peroxidation. Methods Enzymol., *52:* 302-310, 1978.

82 Dixon, M. M., and Kleppe, K. D-Amino acid oxidase. II. Specificity, competitive inhibition and reaction sequence. Biochim. Biophys. Acta, *96:* 368-382, 1965.

83 Goodman, A. I., Choudhury, M., da Silva, J. L., Schwartzman, M. L., and Abraham, N. G. Overexpression of the heme oxygenase gene in renal cell carcinoma. Proc. Soc. Exp. Biol. Med., *214*: 54-61, 1997.

84 Maines, M. D., and Abrahamsson, P. A. Expression of heme oxygenase-1 (HSP32) in human prostate: normal, hyperplastic, and tumor tissue distribution. Urology, *47:* 727-733, 1996.

85 Sahoo, S. K., Sawa, T., Fang, J., Tanaka, S., Miyamoto, Y., Akaike, T., and Maeda, H. Pegylated zinc protoporphyrin: a water-soluble heme oxygenase inhibitor with tumor-targeting capacity. Bioconjugate Chem., *13:* 1031-1038, 2002.

86 Drummond, G. S. Control of heme metabolism by synthetic metalloporphyrins. Ann. N. Y. Acad. Sci. U. S. A., *514:* 87-95, 1987.

87 Abraham, N. G. Quantitation o heme oxygenase (HO-1) copies in human tissues by competitive RT/PCR. *In:* D. Armstrong (ed.), Methods of Molecular Biology, Vol. 108, pp. 199-209, Totowa, NJ: Humana Press Inc., 1998.

88 Royall, J. A., and Ischiropoulos, H. Evaluation of 2', 7'-dichlorofluorescin and dihydrohodamine 123 as fluorescent probes for intracellular H_2O_2 in cultured endothelial cells. Arch. Biochem. Biophys., *302:* 348-355, 1993.

89 Vermes, I., Haanen, C., Steffens-Nakken, H., and Reutelingsperger, C. A novel

assay for apoptosis. Flow cytometric detection of phosphatidylserine expression on early apoptotic cells using fluorescein labeled Annexin V. J. Immunol. Methods. *184:* 39-51, 1995.

90 Elbashir, S. M., Harborth, J., Lendeckel, W., Yalcin, A., Weber, K., and Tuschl, T. Duplexes of 21-nucleotide RNAs mediate RNA interference in cultured mammalian cells. Nature, *411:* 494-498, 2001.

91 Hall, R., and Malia, R. G. Basic haematological practice. *In:* R. Hall, R. G. Malia (ed.), Medical laboratory haematology, 2nd ed., pp. 91-94, 101-104. England: Butterworth-Heinemann Ltd., 1991.

92 Negosecu, A., Lorimier, P., Labat-Moleur, F., Drouet, C., Robert, C., Guillermet, C., Brambilla, C., and Brambilla, E. In situ apoptotic cell labeling by the TUNEL method: improvement and evaluation on cell preparations. J. Histochem. Cytochem., *44:* 959-968, 1996.

93 Cassidy, J., Newell, D. R., Wedge, S. R., Cummings, J. Pharmacokinetics of high molecular weight agents. Cancer Surv., *17:* 315-41, 1993.

94 Lutton, J. D., Abraham, N. G., Drummond, G. S., Levere, R. D., and Kappas, A. Zinc porphyrins: potent inhibitors of hematopoieses in animal and human bone marrow. Proc. Natl. Acad. Sci. U. S. A., *94:* 1432-1436, 1997.

95 Raha, S., and Robinson, B. H. Mitochondria, oxygen free radicals, and apoptosis. Am. J. Med. Genet., *106:* 62-70, 2001.

96 Simon, H. U., Haj-Yehia, A., and Levi-Schaffer, F. Role of reactive oxygen species (ROS) in apoptosis induction. Apoptosis, *5:* 415-418, 2000.

97 Dreher, D., and Junod, A. F. Role of oxygen free radicals in cancer development. Eur. J. Cancer, *32A:* 30-38, 1996.

98 Davies, K. J. Protein modification by oxidants and the role of proteolytic enzymes. Biochem. Soc. Transact., *21:* 346-353, 1993.

99 Lindahl. T. Instability and decay of the primary structure of DNA. Nature, *362:* 709-751, 1993.

100 Demple. B., and Harrison. L. Repair of oxidative damage to DNA: enzymology and biology. Annu. Rev. Biochem., 63: 915-948, 1994.

101 Cerutti. P. A., and Trump, B. F. Inflammation and oxidative stress in carcinogenesis. Cancer Cells, *3:* 1-7, 1991.

102 Guyton, K. Z., and Kensler, T. w. Oxidative mechanisms in carcinogenesis. Brit. Med. Bull, *49:* 523-544, 1993.

103 Feig, D. I., Reid, T. M., and Loeb, L. A. Reactive oxygen species in tumorigenesis. Cancer Res., *54:* 1890s-1894s, 1994.

104 Cerutti, P. A. Oxy-radicals and cancer. Lancet, *344:* 862-863, 1994.

105 Droge. W. Free radicals in the physiological control of cell function. Physiol. Rev., *82:* 47-95, 2002.

106 Estensen, R. D., Levy, M., Klopp, S. J., Galbraith, A. R., Mandel, J. S., Blomquist, J. A., and Watenberg, L. W. N-acetylcysetine suppression of the proliferative index in the colon of patients with previous adenomatous colonic polyps. Cancer Lett., *147:* 109-114, 1999.

107 Greenstein, J. P. Biochemistry of Cancer, 2nd ed. New York: Academic Press, 1954.

108 Hasegawa, Y., Takano, T., Miyauchi, A., Matsuzuka, F., Yoshida, H., Kuma, K., and Amino, N. Decreased expression of glutathione peroxidase mRNA in thyroid anaplastic carcinoma. Cancer Lett. *182:* 69-74, 2002.

109 Yamanaka, N. and Deamer, D. Superoxide dismutase activity in WI-38 cell cultures: effect of age, trypsinization and SV-40 transformation. Physiol. Chem. Phus., *6:* 95-106, 1974.

110 Sato, K., Ito, K., Kohara, H., Yamaguchi, Y., Adachi, K., and Endo, H. Negative regulation of catalase gene expression in hepatoma cells. Mol. Cell. Biol., *12:* 2525-2533, 1992.

111 Nagata, Y., Masui, R., and Akino, T. The presence of free D-serine, D-alanine and D-proline in human plasma. Experientia, *48:* 986-988, 1992.

112 Mates, J. M., Perez-Gomez, C., and Nunez de Castro, I. Antioxidant enzymes and human diseases. Clin Biochem., *32:* 595-603, 1999.

113 Kim, H. S., Lee, T. B., and Choi, C. H. Down-regulation of catalase gene expression in the doxorubicin-resistant AML subline AML-2/DX100. Biochem. Biophys. Res. Commun., *281:* 109-114, 2001.

114 Tanaka, S., Akaike, T., Fang, J., Beppu, T., Ogawa, M., Tamura, F., Miyamoto, Y., and Maeda, H. Antiapoptotic effect of heme oxygenase-1 induced by nitric oxide in experimental solid tumor. Br. J. Cancer, 2003, in press.

115 Lee, T.-S., and Chau, L.-Y. Heme oxygenase-1 mediates the anti-inflammatory effect of interleukin-10 in mice. Nature Med. *8:* 240-246, 2002.

116 Yang, G., Nguyen, X., Ou, J., Rekulapelli, P., Stevenson, D. K., and Dennery, P. A. Unique effects of zinc protoporphyrin on HO-1 induction and apoptosis. Blood, *97:*1306-1313, 2001.

117 Maeda, H. The enhanced permeability and retention (EPR) effect in tumor vasculature: the key role of tumor-selective macromolecular drug targeting. Adv. Enzyme Regul., *41:* 189-207, 2001.

118 Maeda, H., Sawa, T., and Konno, T. Mechanism of tumor-targeted delivery of macromolecular drugs, including the EPR effect in solid tumor and clinical overview of the prototype polymeric drug SMANCS. J. Control. Release, *74:* 47-61, (2001).

119 Tsuruo, T. Mechanisms of multidrug resistance and implications for therapy. Jpn. J. Cancer Res. (Gann), *79:* 285-296, 1988.

120 Wartenberg, M., Ling, F. C., Schallenberg, M., Baumer, A. T., Petrat, K., Hescheler, J., and Sauer, H. Down-regulation of intrinsic P-glycoprotein expression in multicellular prostate tumor spheroids by reactive oxygen species. J. Biol. Chem., *276:* 17420-17428, 2001.

121 Miyamoto, Y., Oda, T., and Maeda, H. Comparison of the cytotoxic effects of the high- and low-molecular-weight anticancer agents on multidrug-resistant Chinese hamster ovary cells in vitro. Cancer Res. *50:* 1571-1575, 1990.

122 Kopecek, J., Kopeckova, P., Minko, T., Lu, Z. R. and Peterson, C. M. Water soluble polymers in tumor targeted delivery. J. Control. Release, *6:* 147-58, 2001.